A First Look at Combining 5π Data Sets

$$\bar{p}p \longrightarrow \pi^+\pi^-\pi^\circ\pi^\circ\pi^\circ$$
$$\bar{p}d \longrightarrow \pi^+\pi^-\pi^-\pi^\circ\pi^\circ p_{\rm spectator}$$
$$\bar{p}d \longrightarrow \pi^-\pi^\circ\pi^\circ\pi^\circ\pi^\circ p_{\rm spectator}$$
$$\bar{p}p \longrightarrow \pi^\circ\pi^\circ\pi^\circ\pi^\circ\pi^\circ$$

Curtis A. Meyer, Ulrike Thoma and Christoph Straßburger

August 12, 1996

1 Introduction

This note is meant to be a summary of our first look at the combined analysis of four 5π data sets: $\bar{p}p \to \pi^+\pi^-\pi^\circ\pi^\circ\pi^\circ$, $\bar{p}n \to \pi^+\pi^-\pi^-\pi^\circ\pi^\circ$, $\bar{p}n \to \pi^-\pi^\circ\pi^\circ\pi^\circ\pi^\circ$, and $\bar{p}p \to \pi^\circ\pi^\circ\pi^\circ\pi^\circ\pi^\circ$. The results are in no way final, but many of the conclusions will be important in the complete analysis. In addition, these analyses indicate which data sets are sensitive to which partial waves, and where it will be safe to extract resonance parameters. At this point in time, our only purpose is to place all the results within a coherent framework. For consistency sake, we have used the same number of data and Monte Carlo events for each sample. This allows a direct comparison of the log–likelyhood. We are currently limited by the size of the $\bar{p}n \to \pi^+\pi^-\pi^-\pi^\circ\pi^\circ$ data set to 11445 data and 19824 Monte Carlo events. These numbers are expected to increase after production of the April '96 data. Finally, not all fits shown in this report have properly converged for all points in the scan — however sufficient point have converged that it is possible to interpolate the true behavior of the functions.

2 An overview of the fitting procedure

.

In the following fits, the mass and width correspond to the mass and total width of the particle. The formulas are derived from K–matrix and T–matrix formulations, but some approximations have been made to allow the fit to work quickly and efficiently. We have tried to follow the formulations in reference [1], although we have made some approximations as indicated.

The F–vector for the production and decay of a resonance as seen in two channels has been written as follows. m_0 is the K–matrix pole, Γ_0 is the total width of the resonance, $\rho_i(m)$ is the phase space factor $2q_i(m)/m^2$ and β is a complex production amplitude which is fit. The

variables $L1$ and $L2$ are the relative L between the two daughter products.

$$\hat{F} = \frac{\beta m_0 \Gamma_0}{{m_0}^2 - m^2 - i m_0 \Gamma_0 ({\gamma_1}^2 \rho_1(m)(B^{L1}(q_1,q_0))^2 + {\gamma_2}^2 \rho_2(m)(B^{L2}(q_2,q_0))^2)} \begin{pmatrix} \gamma_1 B^{L1}(q_1,q_0) \\ \gamma_2 B^{L2}(q_2,q_0) \end{pmatrix}$$

In the case of a particle decaying into $\rho^+\rho^-$ or $(\pi^+\pi^-)_S(\pi^\circ\pi^\circ)_S$, $\sigma\sigma$ we can write the q's as follows:

$$q_{\rho\rho}(m) = \frac{\sqrt{[m^2 - ((m_{\pi+} + m_{\pi^\circ}) + (m_{\pi-} + m_{\pi^\circ}))^2]\,[m^2 - ((m_{\pi+} + m_{\pi^\circ}) - (m_{\pi-} + m_{\pi^\circ}))^2]}}{2m}$$

$$q_{\sigma\sigma}(m) = \frac{\sqrt{[m^2 - ((m_{\pi+} + m_{\pi-}) + (m_{\pi^\circ} + m_{\pi^\circ}))^2]\,[m^2 - ((m_{\pi+} + m_{\pi-}) - (m_{\pi^\circ} + m_{\pi^\circ}))^2]}}{2m}$$

We can now approximate $q_{\rho\rho}$ and $q_{\sigma\sigma}$ as

$$q_{\rho\rho}(m) = \frac{\sqrt{[m^2 - (m_{\pi+} + m_{\pi^\circ} + m_{\pi-} + m_{\pi^\circ})^2]\,[m^2]}}{2m}$$

In the case of a single f_0 decaying to $\rho\rho$ and $\sigma\sigma$, we have $L = 0$ between both the $\rho\rho$ and between the $\sigma\sigma$. This leads to $B^0(q,q_0)$, which is 1. We can now write the F–vector as:

$$\hat{F} = \frac{\beta m_0 \Gamma_0}{{m_0}^2 - m^2 - i m_0 \Gamma_0 \rho(m)} \begin{pmatrix} \gamma_1 \\ \gamma_2 \end{pmatrix}$$

The total transition amplitude can then be written as

$$\mathcal{A} = \hat{F}_{\rho\rho}\hat{T}_\rho\hat{T}_\rho + \hat{F}_{\sigma\sigma}\hat{T}_\sigma\hat{T}_\sigma$$

As an approximation, we sum over the amplitudes $\mathcal{A}$ when introducing additional f_0 resoncances. In reality we should place them within the $\hat{K}$–matrix.

In the case of $\rho' \to \rho\sigma$, we have two possible L values for the decay, 0 and 2. Here we approximate the F–vector by assuming that in the denominator, we can set $\gamma_1^2 = \gamma_2^2 = 0.5$:

$$\hat{F} = \frac{\beta m_0 \Gamma_0}{{m_0}^2 - m^2 - i m_0 \Gamma_0 \rho(m)\,[\gamma_1^2 + \gamma_2^2 (B^2(q,q_0))^2]} \begin{pmatrix} \gamma_1 \\ \gamma_2 B^2(q,q_0) \end{pmatrix}$$

$$\hat{F} \approx \frac{\beta m_0 \Gamma_0}{{m_0}^2 - m^2 - i m_0 \Gamma_0 \rho(m)\,[0.5 + 0.5 (B^2(q,q_0))^2]} \begin{pmatrix} \gamma_1 \\ \gamma_2 B^2(q,q_0) \end{pmatrix}$$

The T–matrix for the decay of $\rho(770) \to \pi\pi$ is given as:

$$\hat{T} = \frac{m_\rho \Gamma_\rho (B^1(q,q_0))^2}{(m_\rho)^2 - m^2 - i m_\rho \Gamma_\rho (2q/m)(B^1(q,q_0))^2}.$$

The variables m_ρ and Γ_ρ are the mass and total width of $\rho(770)$, $B^1(q,q_0)$ is the ratio of Blatt–Weiskopf factors for $L = 1$ and q and q_0 are the decay momenta the ρ. The T–matrix for the $\pi\pi$ S–wave, the σ is taken as the 4–pole solution to the coupled channel analysis of Stefan Spanier [2]. The helicity amplitudes for the channels are as given in reference [3].

3 The Fits

In the fits described below, not all data sets can couple to all channels. In addition, the combinatorics are quite different in the different channels. As such, some of the data sets are more sensitive to features than others. We will present a series of log–likelyhood ($\log \mathcal{L}$) plots. These are produced by holding all masses and widths fixed, and varying the couplings and phases to maximize the $\log \mathcal{L}$. This is then repeated for the 200 points in one of these scans. The $\log \mathcal{L}$ procedure is described in reference [3]. There are several important features to look for in these plots.

- All curves should have the same low–mass and high–mass value. If this is not true, then the fit did not always find the true maximum.
- The large–width ($\Gamma = 1.5$) curve should be smooth, and not vary by a large amount across the plot. If this is not true, it could mean the fit did not converge, or that the amplitude being examined is smaller than some other *unimplemented* amplitude.
- All curves of a given width should be smooth across the plot. If this is not true, then the fit was jumping between local maxima, but probably did not find the true maxima.
- The variation in $\log \mathcal{L}$ is an indication of how important a given contribution is to the entire final state. For a variation to be significant, it must be larger than statistical fluctuations.

We will find that all of the above cases occur during the following fits. In most of the cases it is not important that the true maximum was not always found as it is possible to interpolate to its true position.

Another point to keep in mind is that the four examined final states represent extremely different fractions of the total $\bar{p}N$ annihilation rate. $\bar{p}p \to \pi^+\pi^-\pi^\circ\pi^\circ\pi^\circ$, is nearly 10% of all annihilations, while $\bar{p}p \to \pi^\circ\pi^\circ\pi^\circ\pi^\circ\pi^\circ$ is smaller than 1%. The other two channels fall somewhere in between these. This means that something that is significant in one of the rarer channels may be quite rare in the more common channels.

Finally, in all of these fits, we allow a *flat* background which is incoherent with the remainder of the channel. In principle, we would hope that this is no more than a few percent once a good fit has been achieved. However, as we are attempting to understand a particular channel, the fraction of the data explained by our hypothesis is a good tool to watch.

3.1 Fit 1: $f_0 \to \rho\rho, \sigma\sigma$ and $\rho' \to \rho\sigma$.

We treat this as the reference fit for all following fits. We introduce a single f_0 which is allowed to decay to $\rho\rho$ and $\sigma\sigma$. In addition, we introduce a ρ' which is allowed to decay to $\rho\sigma$. Finally, we allow for a *flat* incoherent background. In the initial scan, we take the values of the $\pi^-\pi^\circ\pi^\circ$ analysis for the ρ', $m = 1.411$ and $\Gamma = 0.343$ [4]. In **table 1** we list the combinatorics which apply to this hypothesis from the 4 data sets.

In **table 2** are summarized the results of this fit. We will take these values as a base line for comparison to later fits. It is interesting that the best $\log \mathcal{L}$ occurs for the most complicated channel. However, this may simply be due to the fact that we include two initial states here, where as we have not included initial P states for deuterium. In addition, the fit to $5\pi^\circ$ only allows a single $f_0 \to \sigma\sigma$.

Combinations	Initial State	Channel
$\bar{p}p \to \pi^+\pi^-\pi^\circ\pi^\circ\pi^\circ$		
6	$^1S_0$	$(\bar{p}N) \to f_0\pi^\circ \to \rho^+\rho^-\pi^\circ$
3	$^1S_0$	$(\bar{p}N) \to f_0\pi^\circ \to \sigma\sigma\pi^\circ$
6	$^1S_0$	$(\bar{p}N) \to \rho'^\pm\pi^\mp \to \rho^\pm\sigma\pi^\mp(L=0)$
6	$^1S_0$	$(\bar{p}N) \to \rho'^\pm\pi^\mp \to \rho^\pm\sigma\pi^\mp(L=2)$
6	$^3S_1$	$(\bar{p}N) \to \rho'^\pm\pi^\mp \to \rho^\pm\sigma\pi^\mp(L=0)$
3	$^3S_1$	$(\bar{p}N) \to \rho'^\circ\pi^\circ \to \rho^\circ\sigma\pi^\circ(L=0)$
6	$^3S_1$	$(\bar{p}N) \to \rho'^\pm\pi^\mp \to \rho^\pm\sigma\pi^\mp(L=2)$
3	$^3S_1$	$(\bar{p}N) \to \rho'^\circ\pi^\circ \to \rho^\circ\sigma\pi^\circ(L=2)$
$\bar{p}n \to \pi^+\pi^-\pi^-\pi^\circ\pi^\circ$		
4	$^1S_0$	$(\bar{p}N) \to f_0\pi^- \to \rho^+\rho^-\pi^-$
2	$^1S_0$	$(\bar{p}N) \to f_0\pi^- \to \sigma\sigma\pi^-$
4	$^1S_0$	$(\bar{p}N) \to \rho'^-\pi^\circ \to \rho^-\sigma\pi^\circ(L=0)$
4	$^1S_0$	$(\bar{p}N) \to \rho'^-\pi^\circ \to \rho^-\sigma\pi^\circ(L=2)$
2	$^1S_0$	$(\bar{p}N) \to \rho'^\circ\pi^- \to \rho^\circ\sigma\pi^-(L=0)$
2	$^1S_0$	$(\bar{p}N) \to \rho'^\circ\pi^- \to \rho^\circ\sigma\pi^-(L=2)$
$\bar{p}n \to \pi^-\pi^\circ\pi^\circ\pi^\circ\pi^\circ$		
3	$^1S_0$	$(\bar{p}N) \to f_0\pi^- \to \sigma\sigma\pi^-$
12	$^1S_0$	$(\bar{p}N) \to \rho'^-\pi^\circ \to \rho^-\sigma\pi^\circ(L=0)$
12	$^1S_0$	$(\bar{p}N) \to \rho'^-\pi^\circ \to \rho^-\sigma\pi^\circ(L=2)$
$\bar{p}p \to \pi^\circ\pi^\circ\pi^\circ\pi^\circ\pi^\circ$		
15	$^1S_0$	$(\bar{p}N) \to f_0\pi^- \to \sigma\sigma\pi^\circ$

Table 1: The combinatorics involved in the four data sets.

Fit	$2\log\mathcal{L}$ $\pi^+\pi^-\pi^\circ\pi^\circ\pi^\circ$	$2\log\mathcal{L}$ $\pi^+\pi^-\pi^-\pi^\circ\pi^\circ$	$2\log\mathcal{L}$ $\pi^-\pi^\circ\pi^\circ\pi^\circ\pi^\circ$	$2\log\mathcal{L}$ $\pi^\circ\pi^\circ\pi^\circ\pi^\circ\pi^\circ$
Fit 1	9000	6000	5000	6775

Table 2: Approximate maximum $\log\mathcal{L}$ for fit 1 in the 4 data sets.

3.1.1 The f_0 Scan

In **figure 1** are presented the $\log\mathcal{L}$ plots for a scan of the mass and width of the f_0 resonance. The peak region of each plot has been expanded in **figure 2**. The mass and width of the ρ' have been held fixed in this plot. Note that the $\bar{p}n \to \pi^+\pi^-\pi^-\pi^\circ\pi^\circ$ data set does not converge in the high–mass limit. This is not important as the peak region is well measured, and we can guess what the high–mass limit should really be.

The common feature of all data sets is that a single f_0 resonance will optimize around the values of the $f_0(1370)$. All four data sets show a structure around a mass of $m = 1.3$ to $m = 1.45$ with a total width between $\Gamma = 0.250$ and $\Gamma = 0.400$. The mass and width are not well determined, but the approximate peak positions are as follows.

- $m = 1.450$, $\Gamma = 0.200$ for $\pi^+\pi^-\pi^\circ\pi^\circ\pi^\circ$.
- $m = 1.350$, $\Gamma = 0.250$ for $\pi^+\pi^-\pi^-\pi^\circ\pi^\circ$.
- $m = 1.400$, $\Gamma = 0.250$ for $\pi^-\pi^\circ\pi^\circ\pi^\circ\pi^\circ$.

- $m = 1.400$, $\Gamma = 0.325$ for $\pi^\circ\pi^\circ\pi^\circ\pi^\circ\pi^\circ$.

With a single f_0 resonance, it seems possible to reproduce the $f_0(1370)$.

Upon closer inspection of the peak region, all of these data hint at two f_0 objects. The clearest evidence comes from $\pi^+\pi^-\pi^-\pi^\circ\pi^\circ$, $\pi^-\pi^\circ\pi^\circ\pi^\circ\pi^\circ$ and $\pi^\circ\pi^\circ\pi^\circ\pi^\circ\pi^\circ$. In all of these cases, there appears to be a double structure, with a narrower object between $m = 1.4$ and $m = 1.5$, and a broader object between $m = 1.3$ and $m = 1.4$. The last thing to point out is that these latter three channels have the largest change in $\log \mathcal{L}$ as we scan mass and widths. All have changes on order 1000, while in $\pi^+\pi^-\pi^\circ\pi^\circ\pi^\circ$, the change is only 200. However, the 0^{++} contribution in the latter is smaller. When we add an additional f_0 in section 3.2, we will fix the mass and width of this first f_0 to $m = 1.325$ and $\Gamma = 0.325$. These are not necessarily the best values, but a good comprimise at this point.

3.1.2 The Background Scan

We can also examine the background plots shown in **figure 3**. We plot the fraction f of the data explained as ρ' plus f_0 as a function of the f_0 mass and width. The background is $b = 1 - f$. Perhaps the most interesting is the $\pi^-\pi^\circ\pi^\circ\pi^\circ\pi^\circ$ data. For extreme values of the f_0, we explain about 42% of the data. When we introduce an f_0 whose mass is between $m = 1.3$ and $m = 1.6$, and whose width is between $\Gamma = 0.100$ and $\Gamma = 0.450$. Then we explain nearly 82% of the data. This striking jump is the clearest evidence on an f_0 in the data.

Next we examine the $\pi^+\pi^-\pi^\circ\pi^\circ\pi^\circ$ and $\pi^\circ\pi^\circ\pi^\circ\pi^\circ\pi^\circ$ data sets. There is an interesting common feature that a broad f_0 of nearly any mass minimizes the background contribution, 20% and 0% respectively. When we choose something like the $f_0(1500)$ parameters, the background rises. The $f_0(1500)$ cannot be the only 0^{++} state in these data. Finally, while the signal in the $5\pi^\circ$ sample varies between 30% and 100%, the variation in $\pi^+\pi^-\pi^\circ\pi^\circ\pi^\circ$ is much smaller, 75% to 80%. The f_0 contribution to the latter is small.

The final plot for $\pi^+\pi^-\pi^-\pi^\circ\pi^\circ$ is a bit more difficult to interpret. First we must discard the high–mass narrow–width points which clearly don't follow the curve. These were exactly the points where the fit had trouble. Then in the region where we saw evidence for our f_0's, we are able to explain about 55 to 60% of the data. However, as we go to certain values of f_0 mass and width, our understanding goes down to about 35%. This indicates that the ρ' does not play as large a role in these data as it does in the $\pi^+\pi^-\pi^\circ\pi^\circ\pi^\circ$ data. In addition, only an $f_0(1500)$ is not going to explain these data.

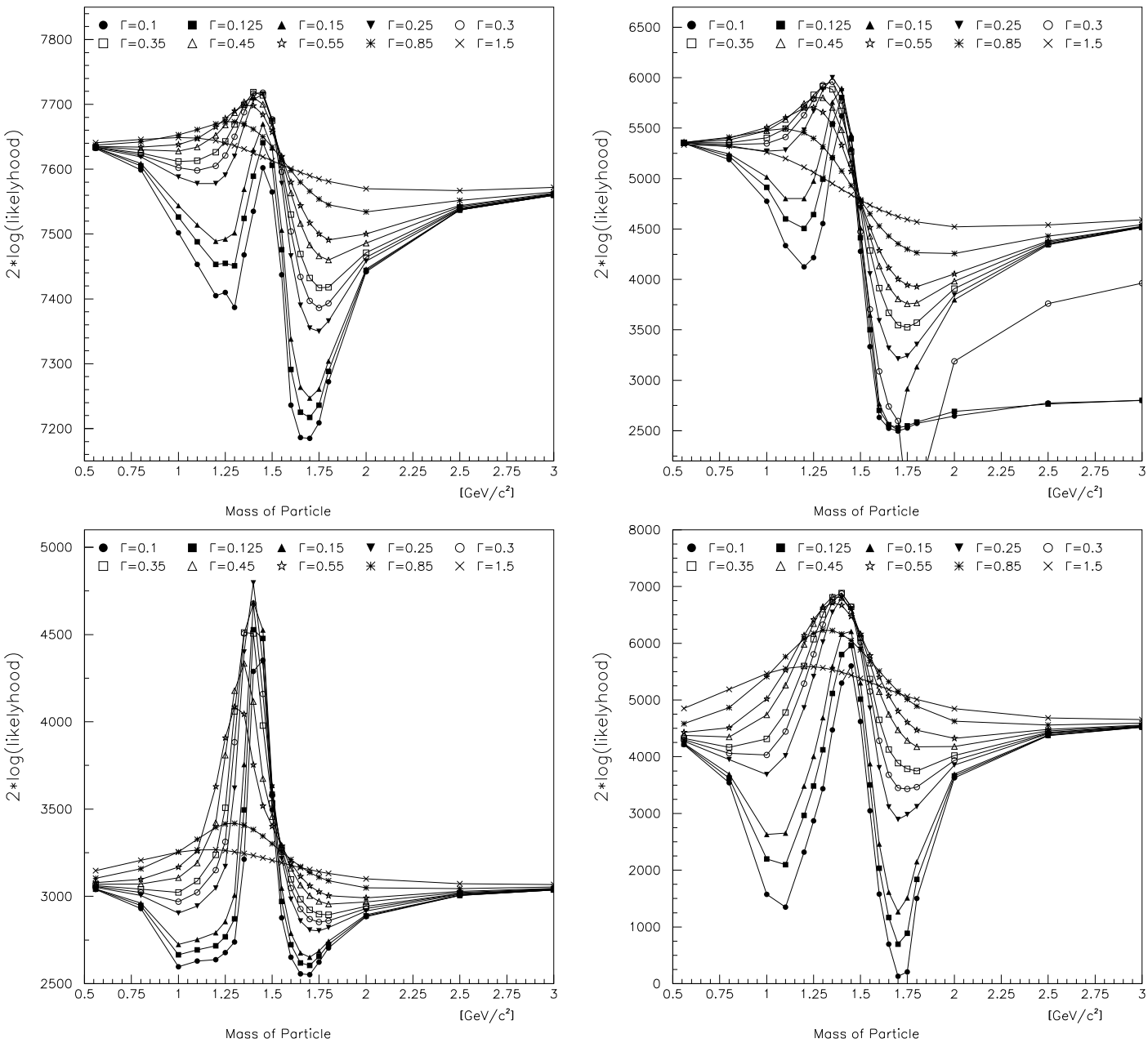

Figure 1: Fix the ρ' at $m = 1.411$, $\Gamma = 0.343$, then scan the mass and width of the single f_0 resonance. **(a)** $\bar{p}p \to \pi^+\pi^-\pi^\circ\pi^\circ\pi^\circ$, **(b)** $\bar{p}n \to \pi^+\pi^-\pi^-\pi^\circ\pi^\circ$, **(c)** $\bar{p}n \to \pi^-\pi^\circ\pi^\circ\pi^\circ\pi^\circ$, and **(d)** $\bar{p}p \to \pi^\circ\pi^\circ\pi^\circ\pi^\circ\pi^\circ$.

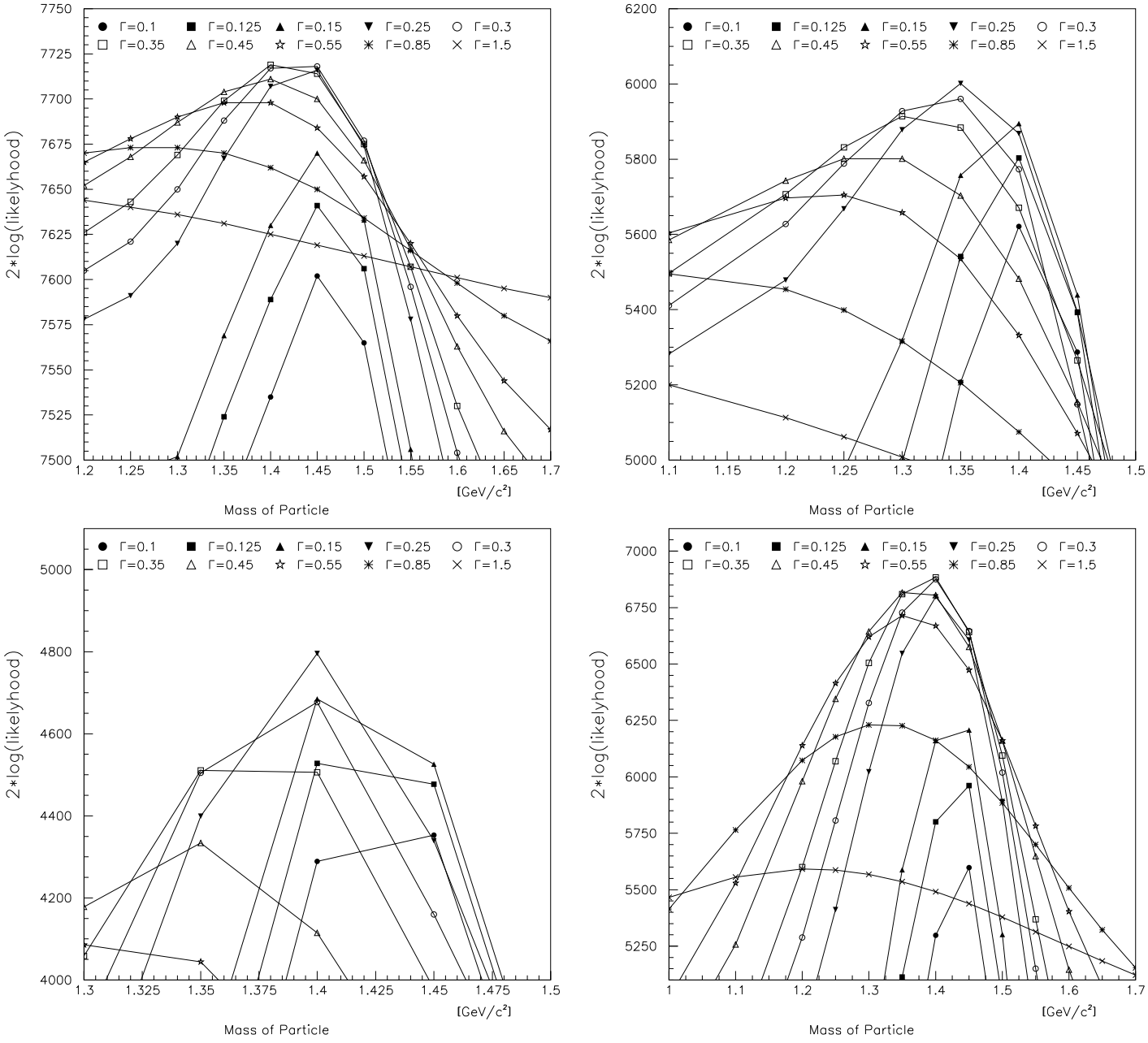

Figure 2: Fix the ρ' at $m = 1.411$, $\Gamma = 0.343$, then scan the mass and width of the single f_0 resonance. **(a)** $\bar{p}p \to \pi^+\pi^-\pi^\circ\pi^\circ\pi^\circ$, **(b)** $\bar{p}n \to \pi^+\pi^-\pi^-\pi^\circ\pi^\circ$, **(c)** $\bar{p}n \to \pi^-\pi^\circ\pi^\circ\pi^\circ\pi^\circ$, and **(d)** $\bar{p}p \to \pi^\circ\pi^\circ\pi^\circ\pi^\circ\pi^\circ$.

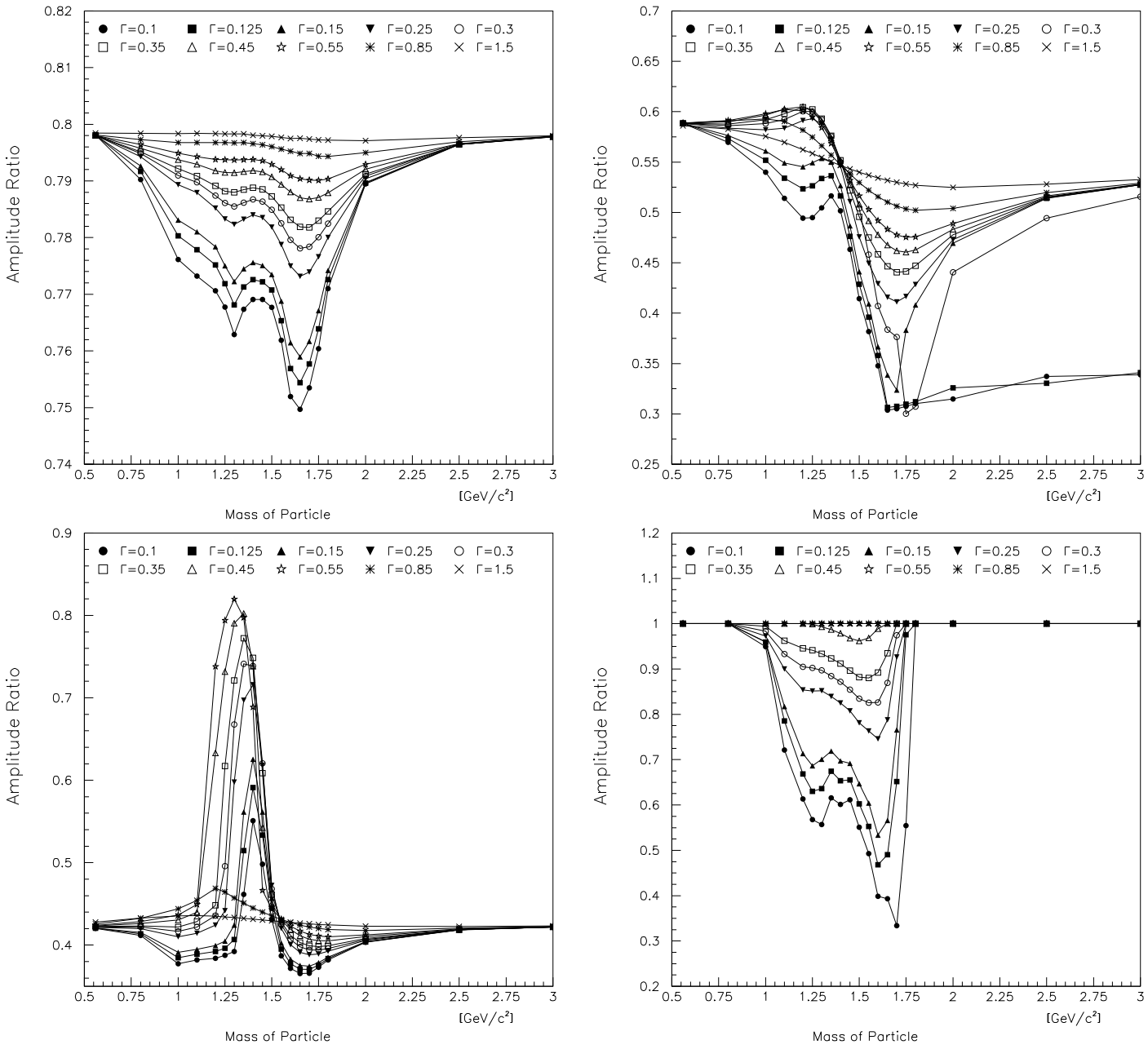

Figure 3: The fraction of data which is explained by the two resonances. Fix the ρ' at $m = 1.411$, $\Gamma = 0.343$, then scan the mass and width of the single f_0 resonance. **(a)** $\bar{p}p \to \pi^+\pi^-\pi^\circ\pi^\circ\pi^\circ$, **(b)** $\bar{p}n \to \pi^+\pi^-\pi^-\pi^\circ\pi^\circ$, **(c)** $\bar{p}n \to \pi^-\pi^\circ\pi^\circ\pi^\circ\pi^\circ$, and **(d)** $\bar{p}p \to \pi^\circ\pi^\circ\pi^\circ\pi^\circ\pi^\circ$.

3.1.3 The ρ' Scan

We will now fix the mass and width of the f_0, and scan the ρ' system. At this point, we have not been entirely consistent in fixing the mass and width. Rather, we have taken something near the maximum of the previous scan. For $\bar{p}p \to \pi^+\pi^-\pi^\circ\pi^\circ\pi^\circ$, we choose $m = 1.500$ and $\Gamma = 0.150$. For the $\bar{p}n \to \pi^+\pi^-\pi^-\pi^\circ\pi^\circ$ data we take $m = 1.500$ and $\Gamma = 0.150$. For the $\bar{p}n \to \pi^-\pi^\circ\pi^\circ\pi^\circ\pi^\circ$ data, we take $m = 1.450$ and $\Gamma = 0.150$. There can be no ρ' in the $5\pi^\circ$ data set. The scans are now shown in **figure 4** and a zoomed view of the peak regions is shown in **figure 5**. The two sharp downward *spikes* in the $\pi^+\pi^-\pi^-\pi^\circ\pi^\circ$ scan are due to the fit jumping to a false maximum, and are not physics. However, one can correctly interpolate where these curves should be by examining the zoomed pictures.

From these plots, the largest change on $\log\mathcal{L}$ is observed in the $\pi^+\pi^-\pi^\circ\pi^\circ\pi^\circ$ data where $\log\mathcal{L}$ ranges over several thousand. It is interesting that there is no clear evidence of peaking in these scans. The fit would rather select a low–mass ρ' — this is the 1^{--} background found in the earlier analysis of $\pi^+\pi^-\pi^\circ\pi^\circ\pi^\circ$ [3]. One should note that all three scans show a structure between $m = 1.3$ and $m = 1.5$ that builds up for smaller widths, and then washes out as we allow the width to become broader. We currently do not completely understand this, but assume that it hints at a ρ' in this mass region, in addition to either a second ρ' or some other intermediate state. For further analysis, we will assume that the is $\rho' \to \rho\sigma$, and fix its mass and width to the values obtained in the $\pi^-\pi^\circ\pi^\circ$ analysis, ($m = 1.411$, $\Gamma = 0.343$). This does not give the best fit, but is not relevant to the remaining fits. A more detailed examination of the ρ' is done in section 3.5.

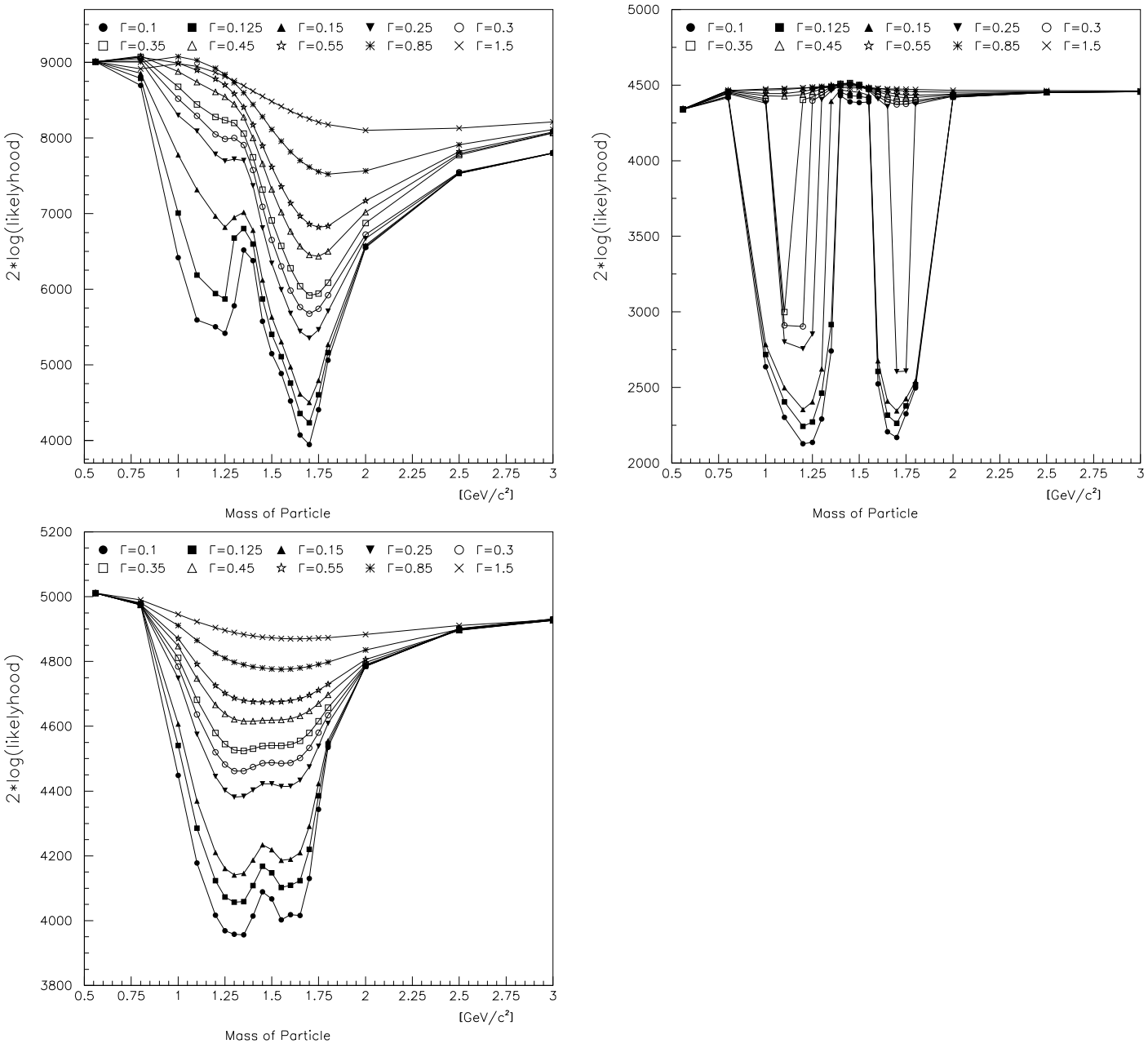

Figure 4: Fix the f_0 at $m = 1.500$, $\Gamma = 0.150$, then scan the mass and width of the ρ' resonance. **(a)** $\bar{p}p \to \pi^+\pi^-\pi^\circ\pi^\circ\pi^\circ$, **(b)** $\bar{p}n \to \pi^+\pi^-\pi^-\pi^\circ\pi^\circ$, and **(c)** $\bar{p}n \to \pi^-\pi^\circ\pi^\circ\pi^\circ\pi^\circ$.

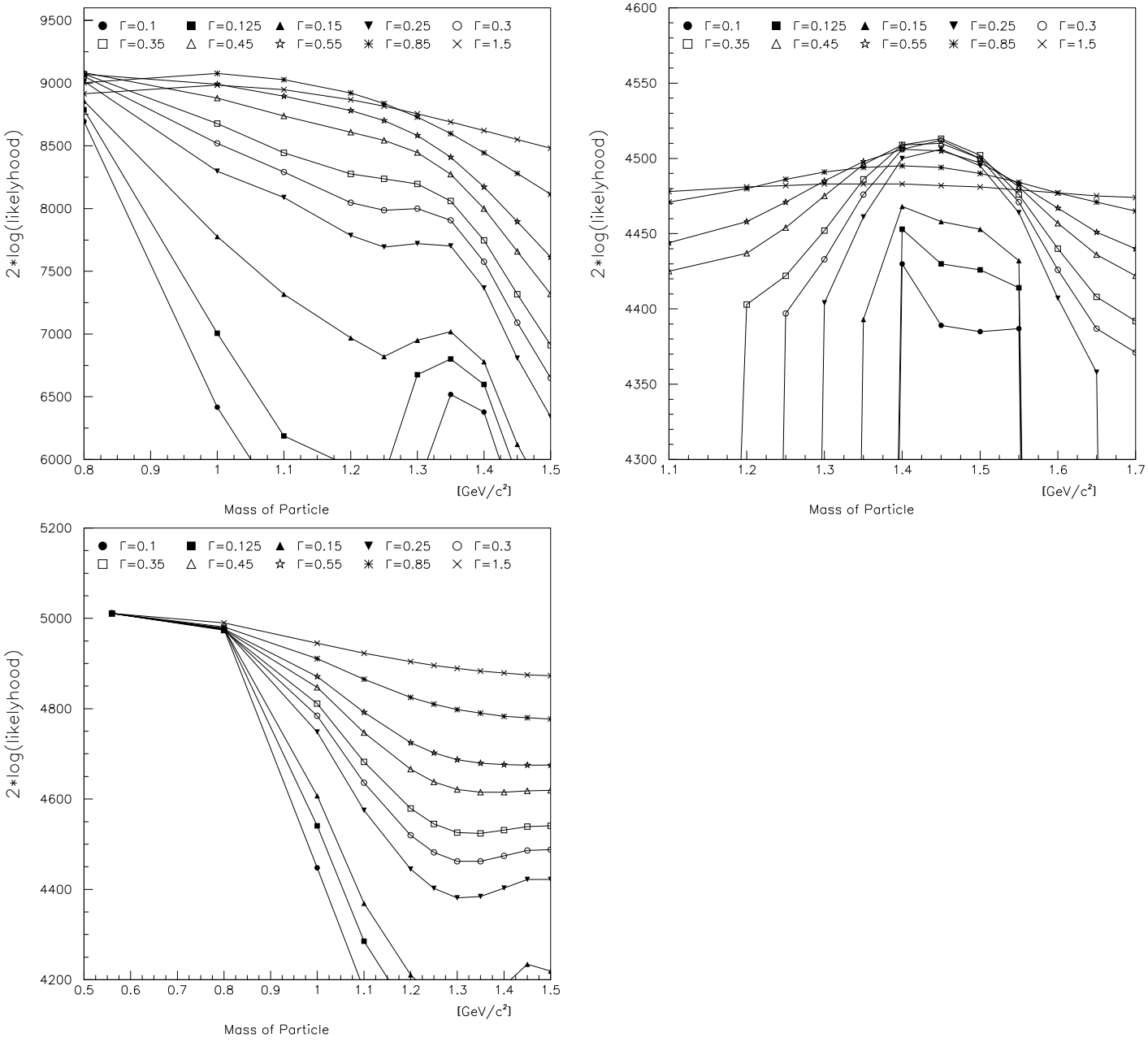

Figure 5: Fix the f_0 at $m = 1.500$, $\Gamma = 0.150$, then scan the mass and width of the ρ' resonance. **(a)** $\bar{p}p \to \pi^+\pi^-\pi^\circ\pi^\circ\pi^\circ$, **(b)** $\bar{p}n \to \pi^+\pi^-\pi^-\pi^\circ\pi^\circ$, and **(c)** $\bar{p}n \to \pi^-\pi^\circ\pi^\circ\pi^\circ\pi^\circ$.

3.2 Fit 2: Two f_0's $\to \rho\rho, \sigma\sigma$ and one $\rho' \to \rho\sigma$.

We will now introduce a second f_0, and study what effect this will have on the fits. The results are summarized in **table 3**, but the $\log \mathcal{L}$ improves by 200 to 600 in all cases. All of these are significant.

Fit	$2\log\mathcal{L}$ $\pi^+\pi^-\pi^\circ\pi^\circ\pi^\circ$	$2\log\mathcal{L}$ $\pi^+\pi^-\pi^-\pi^\circ\pi^\circ$	$2\log\mathcal{L}$ $\pi^-\pi^\circ\pi^\circ\pi^\circ\pi^\circ$	$2\log\mathcal{L}$ $\pi^\circ\pi^\circ\pi^\circ\pi^\circ\pi^\circ$
Fit 1	9000	6000	5000	6775
Fit 2	9200	6550	5170	7150
$\Delta 2\log\mathcal{L}$	200	550	170	375

Table 3: Approximate maximum $\log\mathcal{L}$ for fit 1 and 2 in the four data sets.

3.2.1 The $f_0(1500)$ Scan

To begin we will fix the mass and width of one of the f_0's to $m = 1.325$ and $\Gamma = 0.325$ and the mass and width of the ρ' to $m = 1.411$ and $\Gamma = 0.343$. We then scan the mass and width of the second f_0. The results of these scans are shown in **figure 6** and the zoom view of the peak region are shown in **figure 7**. All sets show a peak in $\log\mathcal{L}$ near $m = 1.5$ and $\Gamma = 0.150$. For the $\pi^+\pi^-\pi^\circ\pi^\circ\pi^\circ$ data we will read the mass and width **figure 17** where we have used roughly 3.5 times the current statistics.

Sample	Mass	Width	$\Delta(2\log\mathcal{L})$
$\pi^+\pi^-\pi^\circ\pi^\circ\pi^\circ$	$m = 1.500$	$\Gamma = 0.200$	30
$\pi^+\pi^-\pi^-\pi^\circ\pi^\circ$	$m = 1.550$	$\Gamma = 0.150$	150
$\pi^-\pi^\circ\pi^\circ\pi^\circ\pi^\circ$	$m = 1.500$	$\Gamma = 0.140$	900
$\pi^\circ\pi^\circ\pi^\circ\pi^\circ\pi^\circ$	$m = 1.450$	$\Gamma = 0.125$	350

Table 4: Optimum values for the $f_0(1500)$ in fit 2.

We summarize the results in **table 4**. First all of these results are all consistent with $m = 1.5$ and $\Gamma = 0.150$ and we will then take these latter values as the mass and width of the second f_0 resonance. Several of these plots indicate that the mass and width of the first f_0 are wrong, or that we might need a third f_0. In particular, as the width of the second f_0 is increased, we note that the mass of the peak has a tendency to shift towards lower values. This is most clear in $\pi^\circ\pi^\circ\pi^\circ\pi^\circ\pi^\circ$ where the peak goes to about $m = 1.1$ with the largest width. In order to settle this question, we will want to fix the mass of the $f_0(1500)$, and scan the mass of the other f_0. This will be attempted in section 3.2.3.

We can however perform some checks here by choosing different masses and widths for the first f_0. In **figure 8** we show two plots. The first has an f_0 fixed at $m = 1.1$ and $\Gamma = 0.900$, the second has an f_0 fixed at $m = 1.25$ and $\Gamma = 0.600$. We can draw on very important conclusion here — regardless of the choice of $f_0(1300)$ mass and width within a wide range that most of us would consider reasonable, the $f_0(1500)$ parameters are **stable** and the contribution is **significant**. We do not need to clearly see the $f_0(1300)$ to understand the $f_0(1500)$ in this data set.

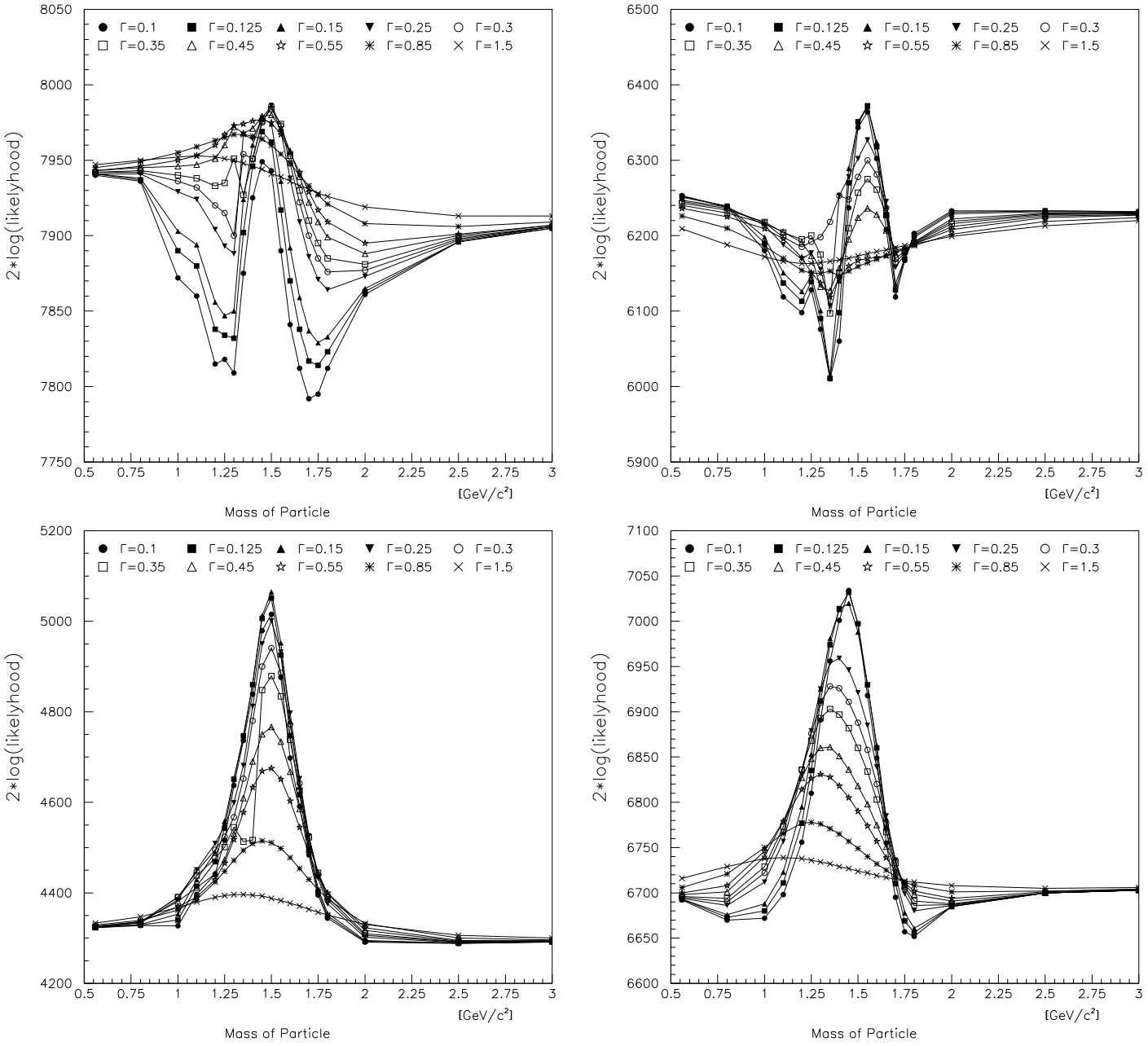

Figure 6: Fix the ρ' at $m = 1.411$, $\Gamma = 0.343$, the first f_0 to $m = 1.325$ and $\Gamma = 0.325$ and then scan the mass and width of the second f_0 resonance. **(a)** $\bar{p}p \to \pi^+\pi^-\pi^\circ\pi^\circ\pi^\circ$, **(b)** $\bar{p}n \to \pi^+\pi^-\pi^-\pi^\circ\pi^\circ$, **(c)** $\bar{p}n \to \pi^-\pi^\circ\pi^\circ\pi^\circ\pi^\circ$, and **(d)** $\bar{p}p \to \pi^\circ\pi^\circ\pi^\circ\pi^\circ\pi^\circ$.

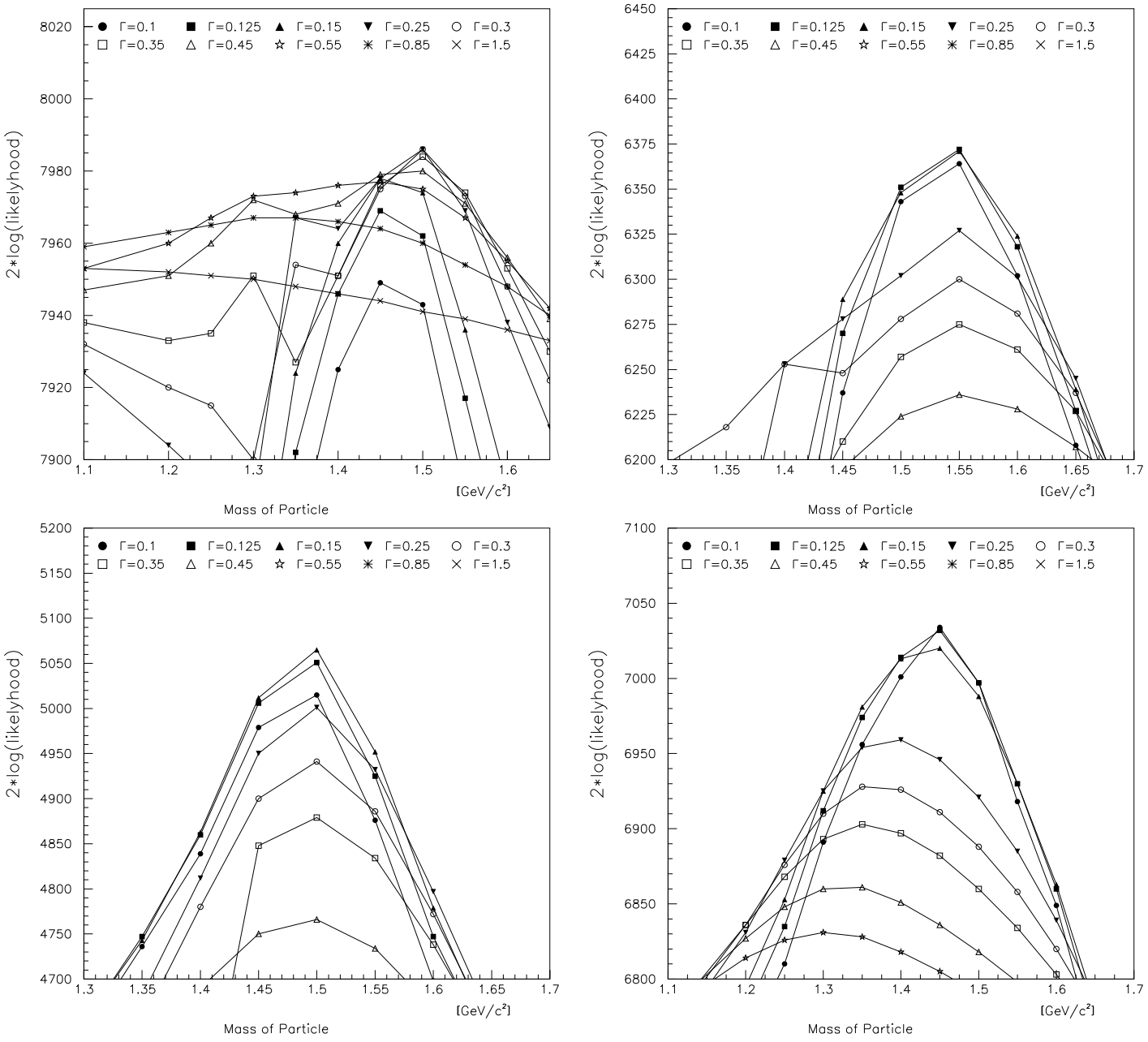

Figure 7: Fix the ρ' at $m = 1.411$, $\Gamma = 0.343$, then scan the mass and width of the second f_0 resonance. **(a)** $\bar{p}p \to \pi^+\pi^-\pi^\circ\pi^\circ\pi^\circ$, **(b)** $\bar{p}n \to \pi^+\pi^-\pi^-\pi^\circ\pi^\circ$, **(c)** $\bar{p}n \to \pi^-\pi^\circ\pi^\circ\pi^\circ\pi^\circ$, and **(d)** $\bar{p}p \to \pi^\circ\pi^\circ\pi^\circ\pi^\circ\pi^\circ$.

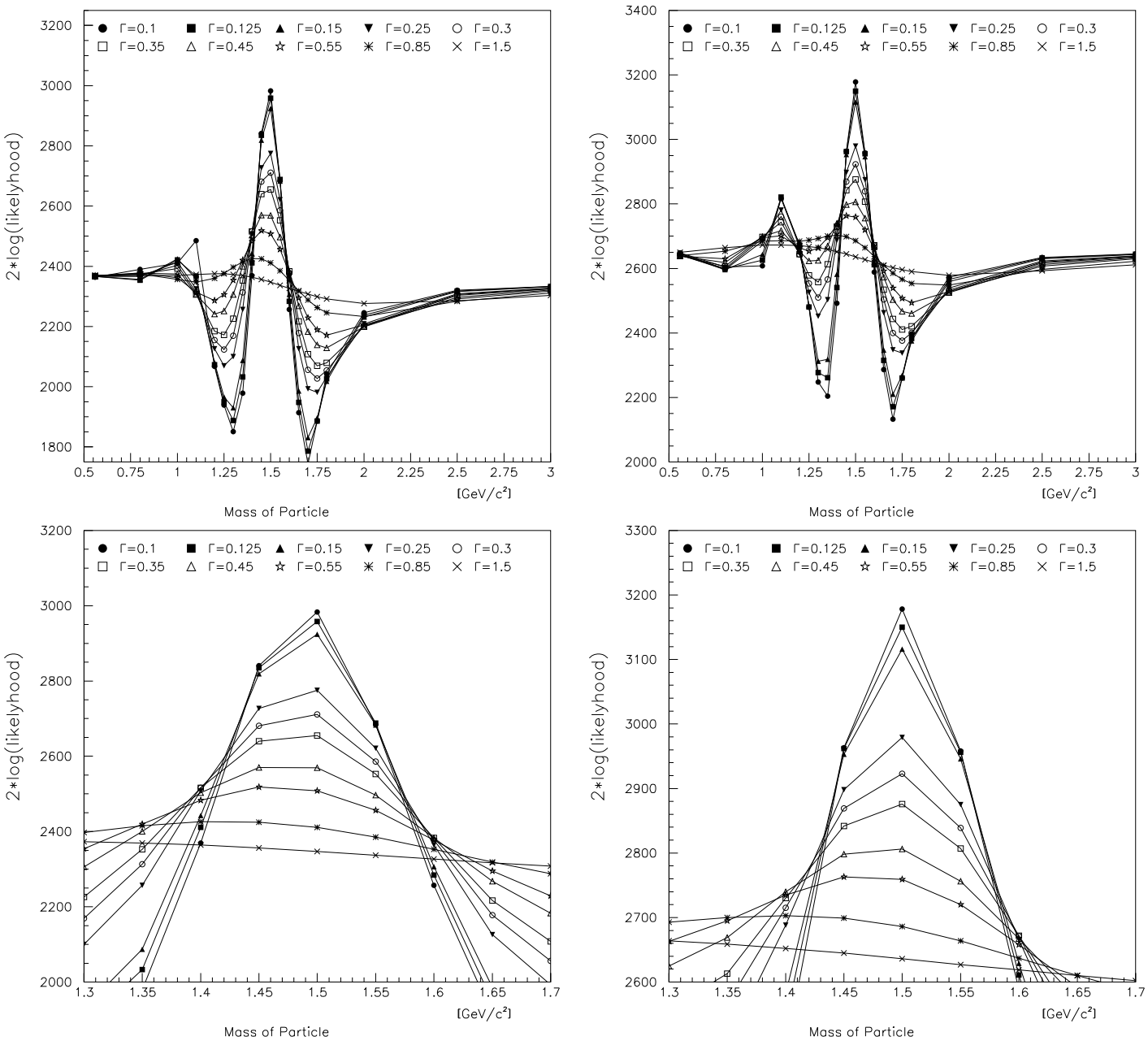

Figure 8: Fix the ρ' at $m = 1.411$, $\Gamma = 0.343$ and examine the $\pi^-\pi^\circ\pi^\circ\pi^\circ\pi^\circ$ data. In **(a)** and **(c)** the first f_0 has been held fixed at $m = 1.1$ and $\Gamma = 0.900$. In **(b)** and **(d)** we hold the first f_0 fixed at $m = 1.25$ and $\Gamma = 0.600$. We then scan the mass and width of the $f_0(1500)$.

3.2.2 The $\rho'(1450)$ Scan

We now fix the mass and width of the first f_0's to $m = 1.325$ and $\Gamma = 0.325$ and the mass and width of the second f_0 to $m = 1.500$ and $\Gamma = 0.150$. We then scan the mass and width of the ρ'. The results of these scans are shown in **figure 9** and the zoom view of the peak region are shown in **figure 10**. As before there is no strong peaking of $\log \mathcal{L}$, but the data still hint at a buried ρ' around $m = 1.3$ to $m = 1.4$. We will continue to retain $m = 1.411$ and $\Gamma = 0.343$ for the ρ' even though this is clearly not the best choice. We will return to this problem in section 3.5.

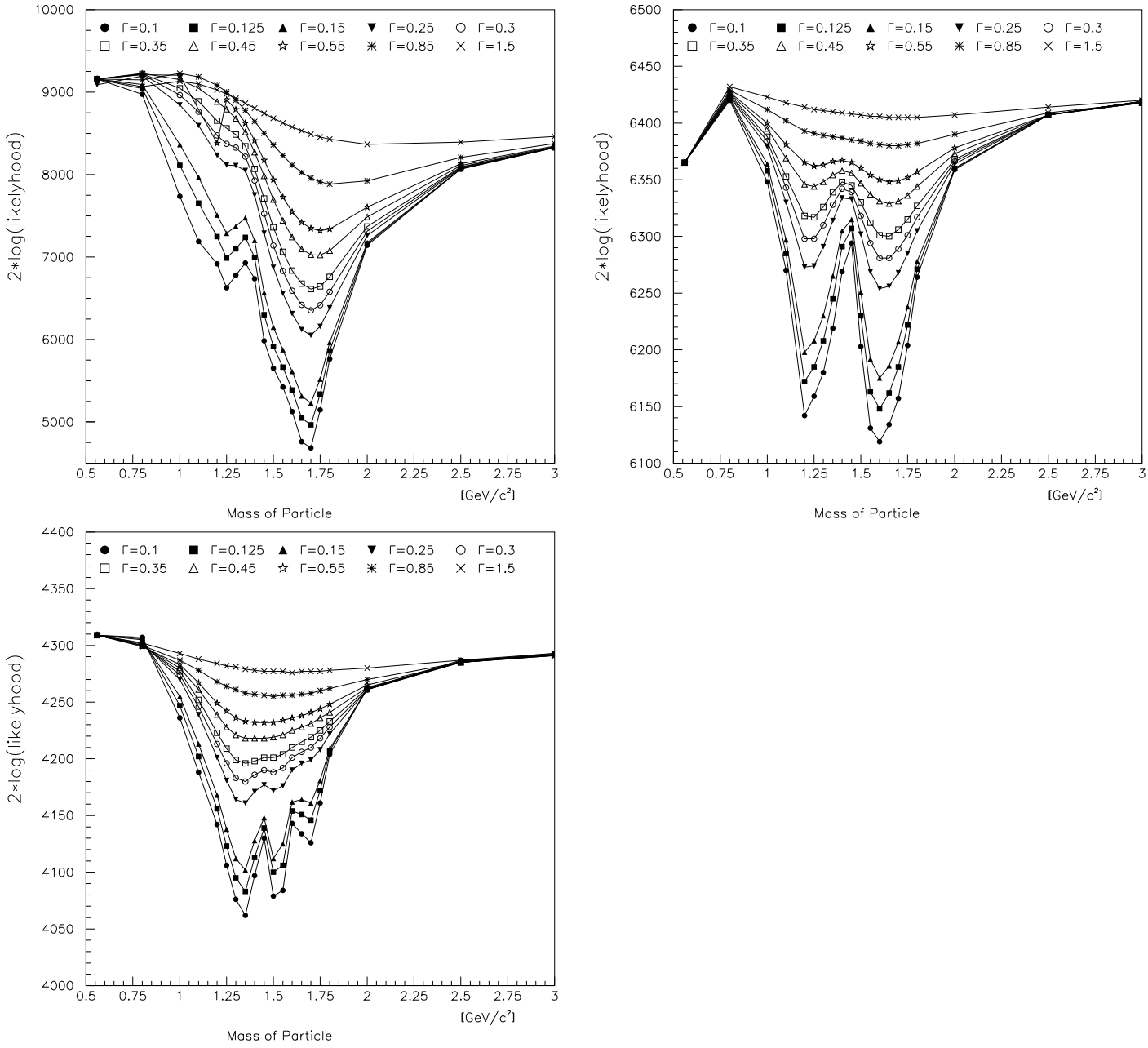

Figure 9: Fix the masses and widths for the two f_0's at $m = 1.325$, $\Gamma = 0.325$, and $m = 1.500$, $\Gamma = 0.150$. Scan the mass and width of the ρ' resonance. **(a)** $\bar{p}p \to \pi^+\pi^-\pi^\circ\pi^\circ\pi^\circ$, **(b)** $\bar{p}n \to \pi^+\pi^-\pi^-\pi^\circ\pi^\circ$, **(c)** $\bar{p}n \to \pi^-\pi^\circ\pi^\circ\pi^\circ\pi^\circ$, and **(d)** $\bar{p}p \to \pi^\circ\pi^\circ\pi^\circ\pi^\circ\pi^\circ$.

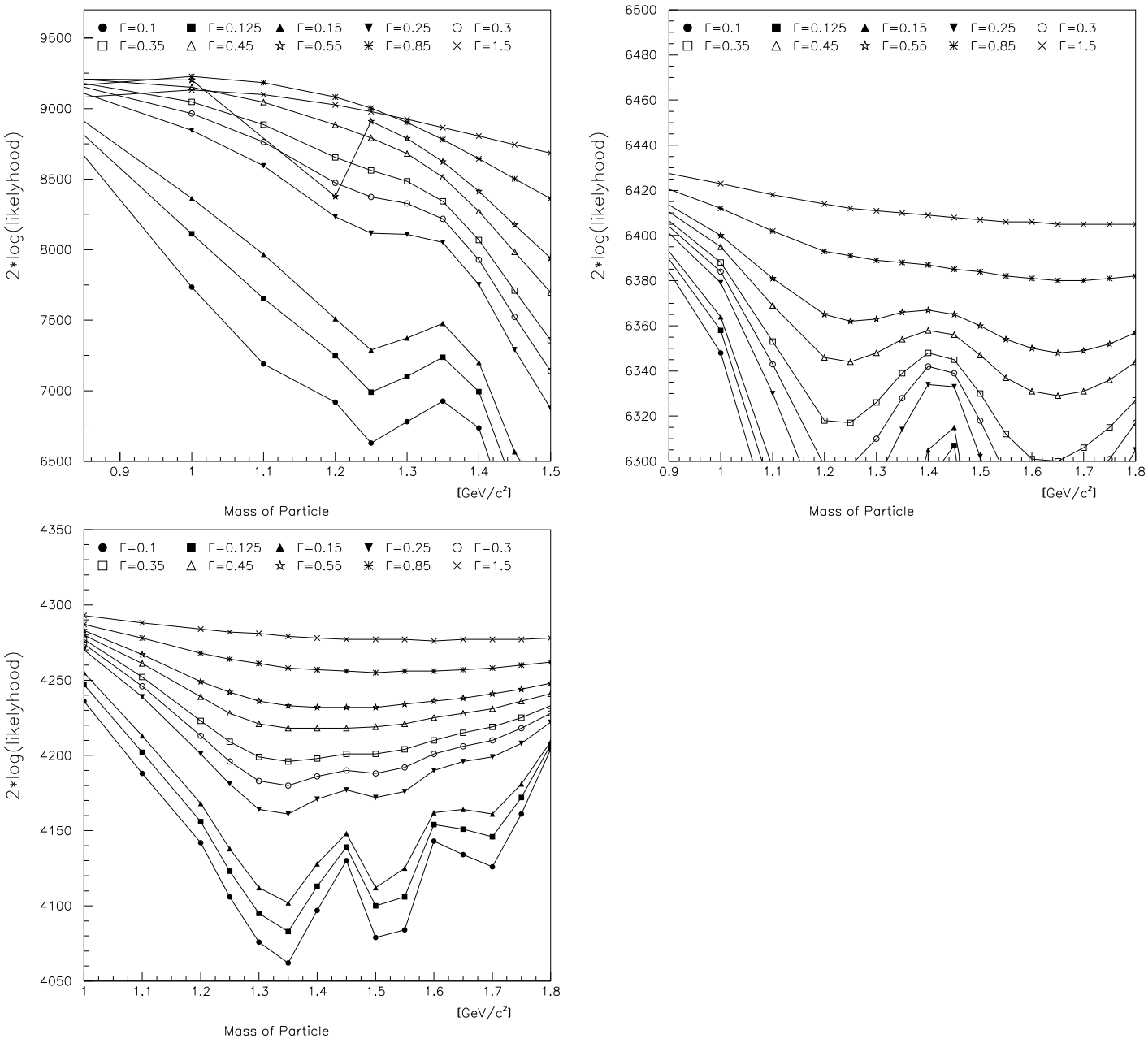

Figure 10: Fix the masses and widths for the two f_0's at $m = 1.325$, $\Gamma = 0.325$, and $m = 1.500$, $\Gamma = 0.150$. Scan the mass and width of the ρ' resonance. **(a)** $\bar{p}p \to \pi^+\pi^-\pi^\circ\pi^\circ\pi^\circ$, **(b)** $\bar{p}n \to \pi^+\pi^-\pi^-\pi^\circ\pi^\circ$, **(c)** $\bar{p}n \to \pi^-\pi^\circ\pi^\circ\pi^\circ\pi^\circ$, and **(d)** $\bar{p}p \to \pi^\circ\pi^\circ\pi^\circ\pi^\circ\pi^\circ$.

3.2.3 The $f_0(1325)$ Scan

Here we have fixed the mass and width of the second f_0 to $m = 1.500$, $\Gamma = 0.150$, and the mass and width of the ρ' to $m = 1.411$, $\Gamma = 0.343$. We then scan the first f_0. The results are shown in **figure 11** and the zoomed views are shown in **figure 12**. We also plot the signal fractions in **figure 13**. First of all we observe that all four of these fits are unstable. This is probably coupled to the small statistics as discussed in section 3.4. However, we can still attempt to draw some conclusions from this scan. First the $\pi^+\pi^-\pi^\circ\pi^\circ\pi^\circ$ data are not very sensitive to this second f_0, with the optimum value found at low mass and broad widths. The data are suggestive of a structure in the $m = 1.3$ region which is washed out as we scan. The $\pi^+\pi^-\pi^-\pi^\circ\pi^\circ$ and $\pi^-\pi^\circ\pi^\circ\pi^\circ\pi^\circ$ data also want to push the mass to a *low* value, and select a broad width. In fact the preferred value is the lower mass limit, which is just a background term. There is some hint in $\pi^+\pi^-\pi^-\pi^\circ\pi^\circ$ of a shoulder at $m = 1.2$ to $m = 1.3$ with a width of $\Gamma = 0.250$ to $\Gamma = 0.550$. In the $\pi^-4\pi^\circ$ sample, there is a hint of the washed out structure noted above. Until the background is understood we are unable to accurately extract the mass and width of this second f_0. We may very well need three poles, one of which is quite broad. Finally, the $\pi^\circ\pi^\circ\pi^\circ\pi^\circ\pi^\circ$ data show a broad f_0 with a mass of about $m = 1.2$. However, this is not a very significant peak. Any mass value between $m = 0.9$ and $m = 1.4$, with a width between $\Gamma = 0.400$ to $\Gamma = 1.500$ would give nearly the same fit.

Next, let us examine the signal fraction as shown in **figure 13**. As we saw in fit 1, the $\pi^+\pi^-\pi^\circ\pi^\circ\pi^\circ$ data are not very sensitive to this second f_0. The signal is typically 78% of the data. The $\pi^+\pi^-\pi^-\pi^\circ\pi^\circ$ data show an interesting effect. Using a very broad f_0 would require a 40% background contribution. This is als true for a very light or very heavy f_0. In these cases the tail of such an object tend to explain part of the broad background. Finally, for masses around $m = 1.5$, and narrowish widths, we need 55% background. Essentially, we are not explaining the broad flat background. Next, the $\pi^-\pi^\circ\pi^\circ\pi^\circ\pi^\circ$ data show us that for a light f_0, we can explain 70% of the data. With only an $f_0(1500)$ we accommodate about 50% of the data, and oddly, a high–mass f_0 parametrizes the background worse than the low–mass one, explaining only 60% of the data. Finally the $5\pi^\circ$ data again show us that with a very broad f_0, we can explain about 100% of the data. With any other combination, we need between 5% and 25% background.

The role this second f_0 appears to be playing is two–fold. The fit is trynig to use a broad f_0, or the extreme tails of an f_0 to explain the background. Additionally, the fit is trying to explain a broad, but presumably weak object in the range of $m = 1.1$ to $m = 1.4$. In order to unravel this, a more complicated analysis will need to be performed.

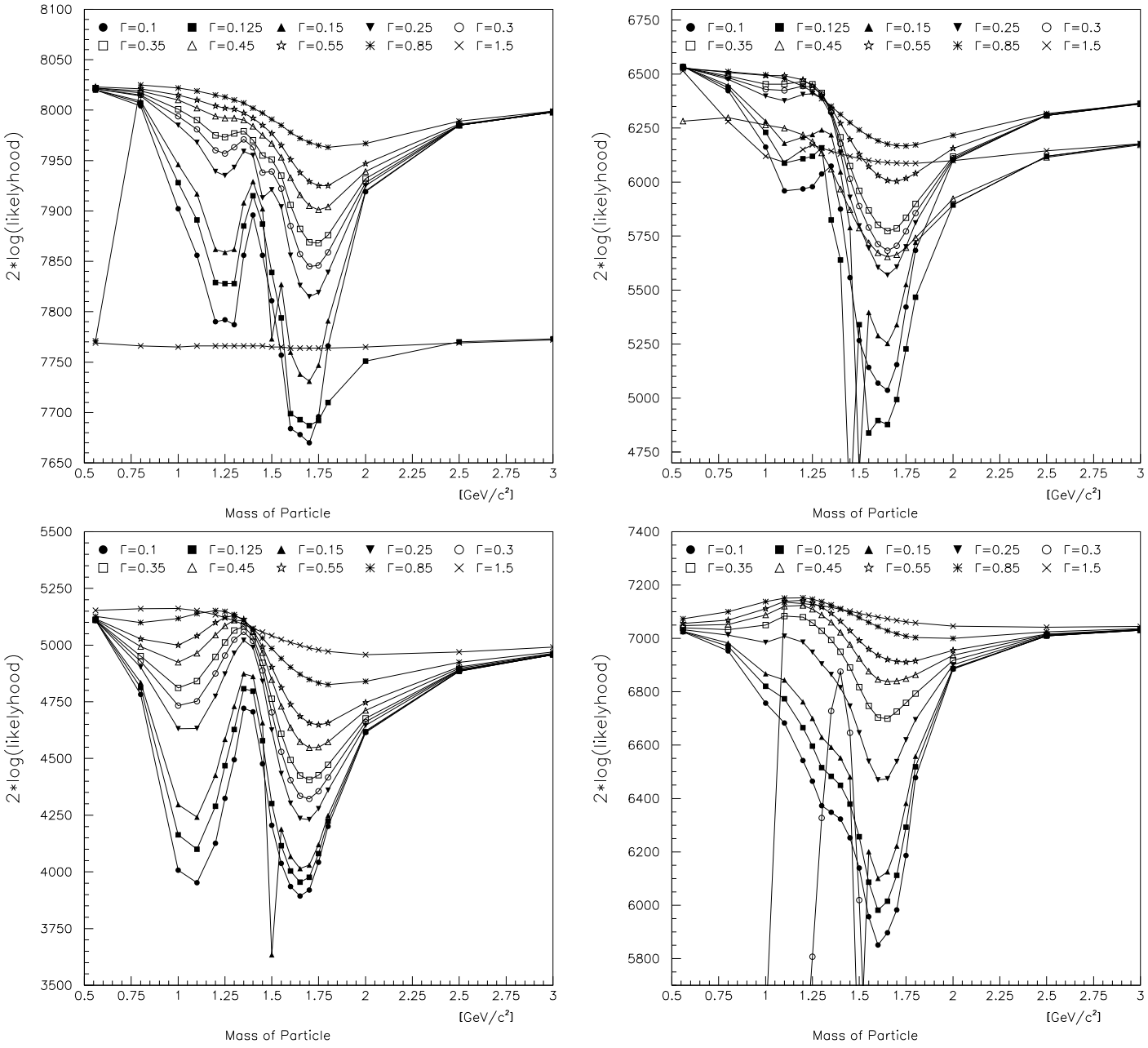

Figure 11: Fix the ρ' at $m = 1.411$, $\Gamma = 0.343$, the second f_0 to $m = 1.500$ and $\Gamma = 0.150$ and then scan the mass and width of the first f_0 resonance. **(a)** $\bar{p}p \to \pi^+\pi^-\pi^\circ\pi^\circ\pi^\circ$, **(b)** $\bar{p}n \to \pi^+\pi^-\pi^-\pi^\circ\pi^\circ$, **(c)** $\bar{p}n \to \pi^-\pi^\circ\pi^\circ\pi^\circ\pi^\circ$, and **(d)** $\bar{p}p \to \pi^\circ\pi^\circ\pi^\circ\pi^\circ\pi^\circ$.

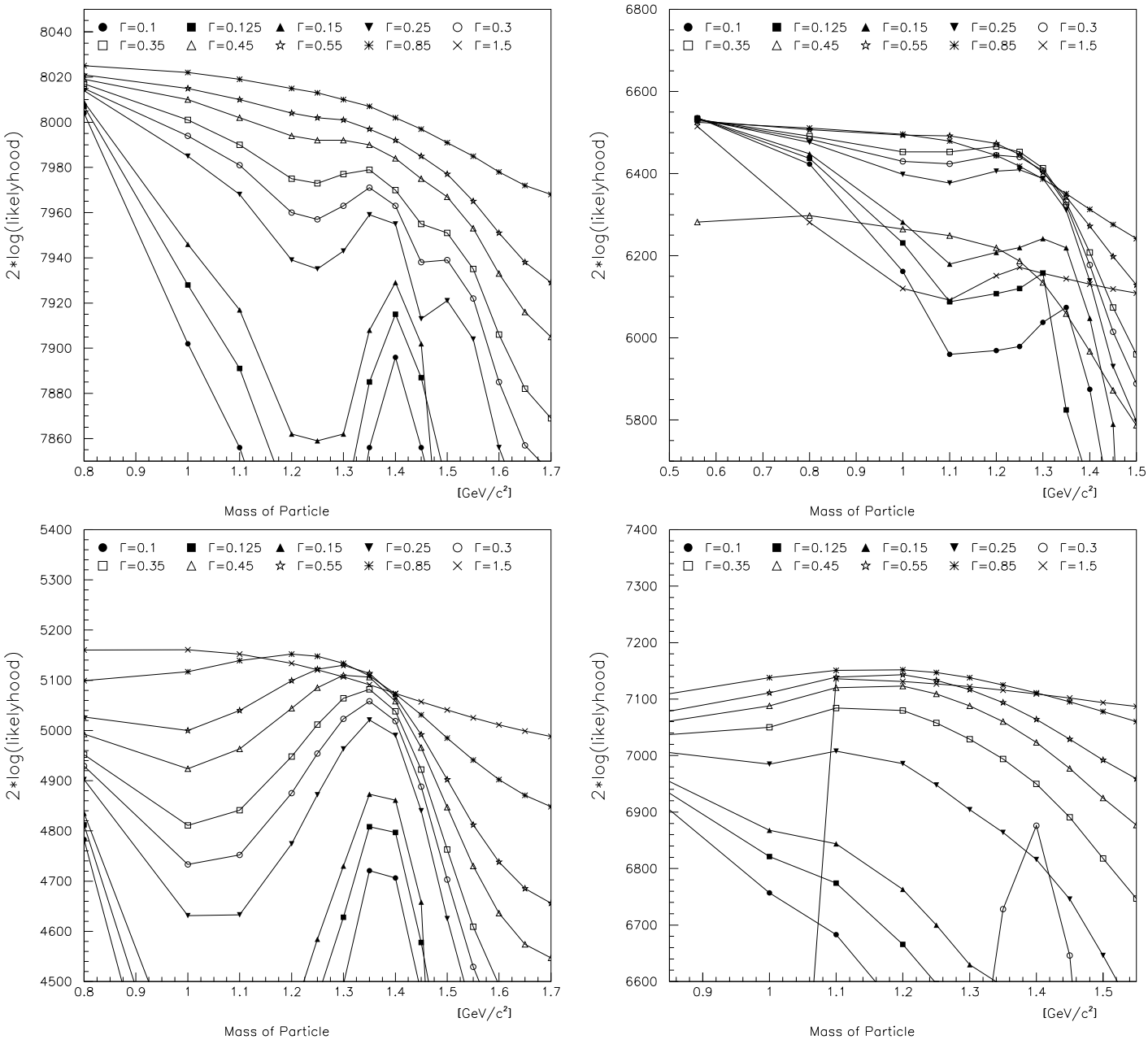

Figure 12: Fix the ρ' at $m = 1.411$, $\Gamma = 0.343$, the second f_0 to $m = 1.500$ and $\Gamma = 0.150$ and then scan the mass and width of the mass and width of the first f_0 resonance. **(a)** $\bar{p}p \to \pi^+\pi^-\pi^\circ\pi^\circ\pi^\circ$, **(b)** $\bar{p}n \to \pi^+\pi^-\pi^-\pi^\circ\pi^\circ$, **(c)** $\bar{p}n \to \pi^-\pi^\circ\pi^\circ\pi^\circ\pi^\circ$, and **(d)** $\bar{p}p \to \pi^\circ\pi^\circ\pi^\circ\pi^\circ\pi^\circ$.

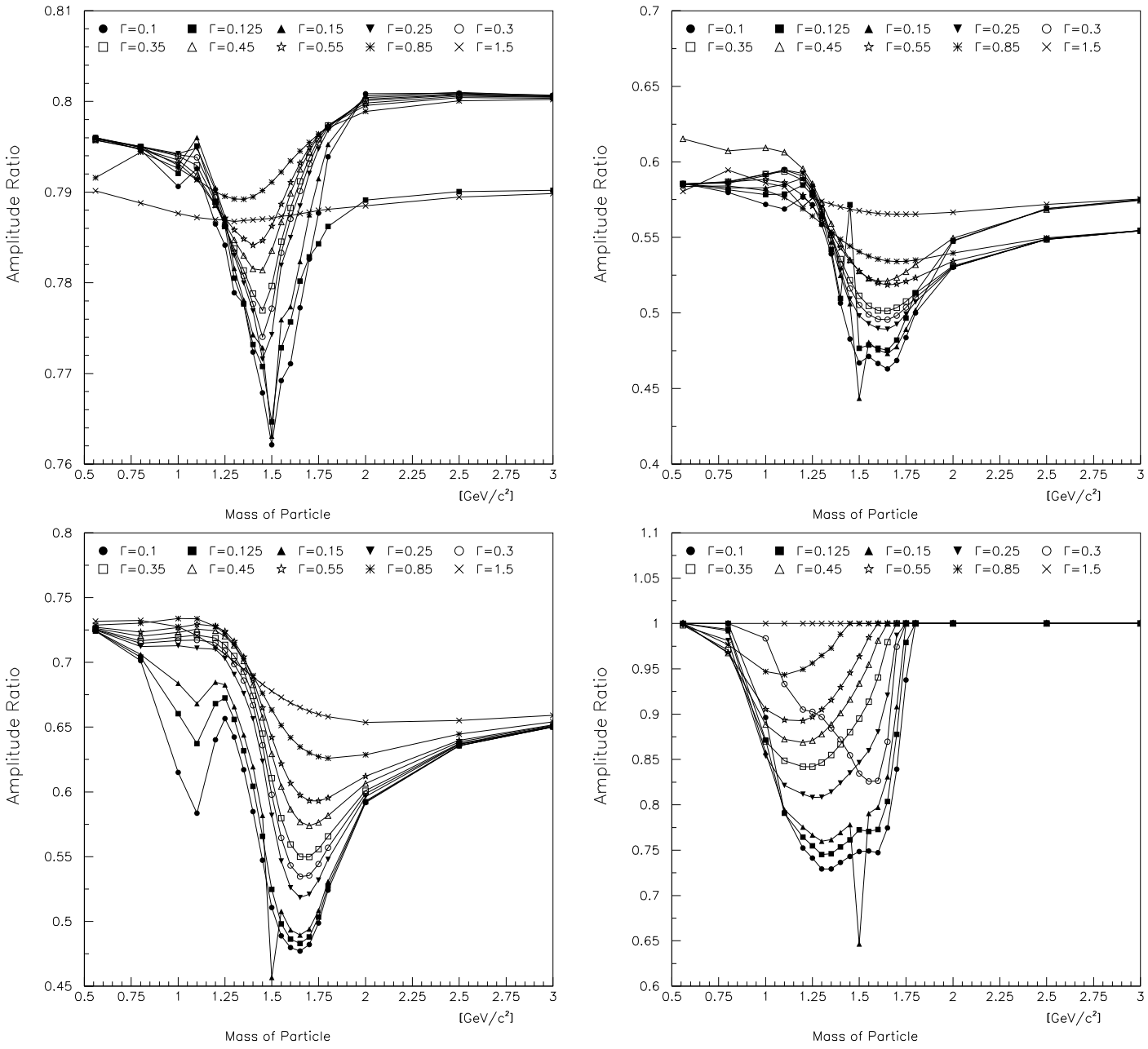

Figure 13: The fraction of data which is explained by the three resonances. Fix the ρ' at $m = 1.411$, $\Gamma = 0.343$, the second f_0 to $m = 1.500$, $\Gamma = 0.150$ and then scan the mass and width of the first f_0 resonance. **(a)** $\bar{p}p \to \pi^+\pi^-\pi^\circ\pi^\circ\pi^\circ$, **(b)** $\bar{p}n \to \pi^+\pi^-\pi^-\pi^\circ\pi^\circ$, **(c)** $\bar{p}n \to \pi^-\pi^\circ\pi^\circ\pi^\circ\pi^\circ$, and **(d)** $\bar{p}p \to \pi^\circ\pi^\circ\pi^\circ\pi^\circ\pi^\circ$.

3.2.4 The $\rho(770)$ Scan

It is also possible to check the mass and width of the $\rho(770)$. In these fits, we have fixed the parameters of the first f_0 to $m = 1.325$, $\Gamma = 0.325$, the second f_0 to $m = 1.500$, $\Gamma = 0.325$ and the parameters of the ρ' to $m = 1.411$, $\Gamma = 0.343$. We then scan the mass and width of the $\rho(770)$ for values near the expected mass and width. The results are shown in **figure 14** and a zoomed view in **figure 14**. This is currently a disturbing point of this analysis, especially the result from $\pi^+\pi^-\pi^-\pi^\circ\pi^\circ$ which shows no maximum in the $\rho(770)$ parameters, and is currently not understood. It will be important to reproduce reasonable values for the $\rho(770)$ in any final fit.

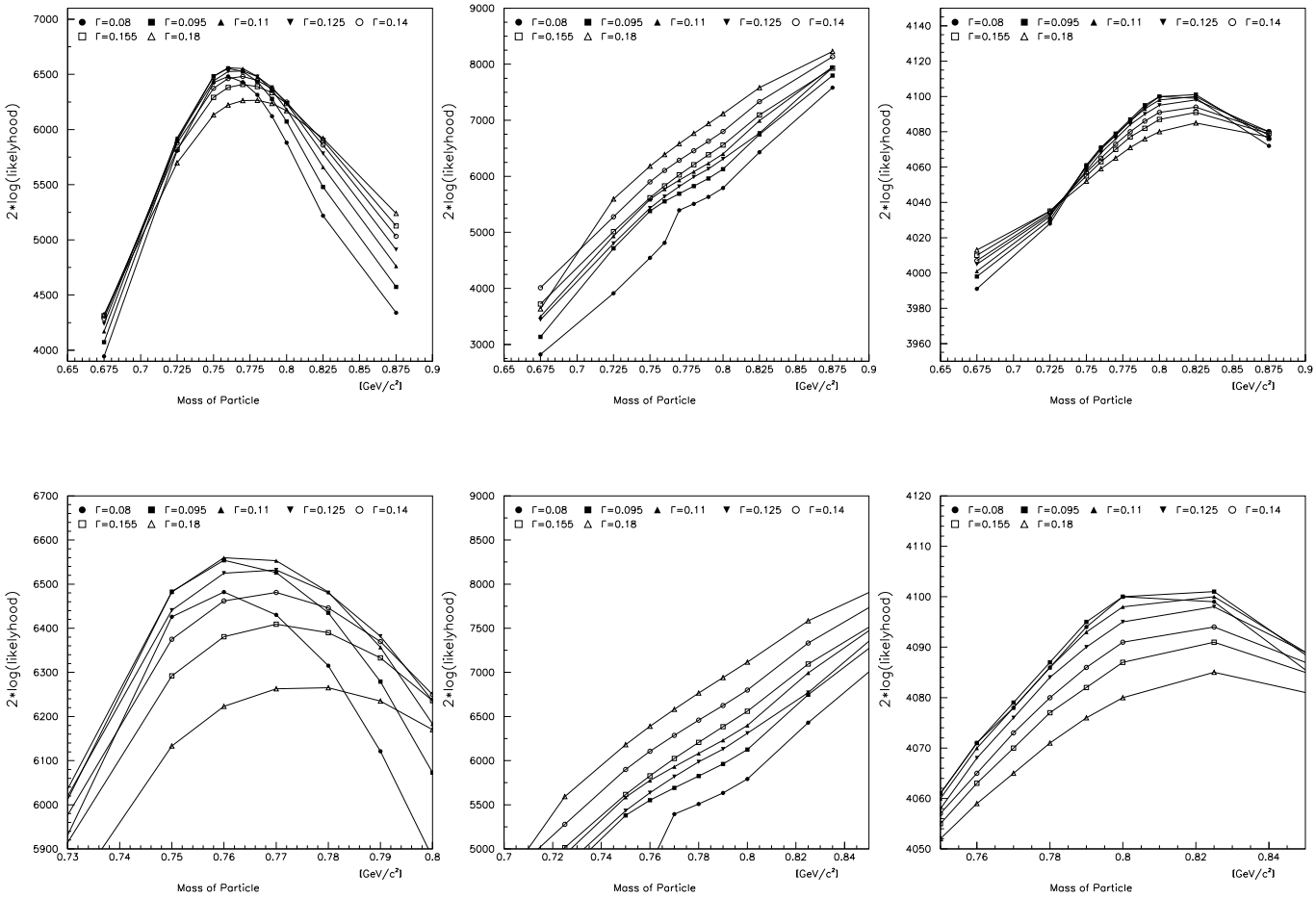

Figure 14: Fix the ρ' at $m = 1.411$, $\Gamma = 0.343$, the first f_0 to $m = 1.325$ and $\Gamma = 0.325$ and the second f_0 to $m = 1.500$ and $\Gamma = 0.150$ and then scan the mass and width of the $\rho(770)$. **(a)** $\bar{p}p \to \pi^+\pi^-\pi^\circ\pi^\circ\pi^\circ$, **(b)** $\bar{p}n \to \pi^+\pi^-\pi^-\pi^\circ\pi^\circ$ and **(c)** $\bar{p}n \to \pi^-\pi^\circ\pi^\circ\pi^\circ\pi^\circ$. **d**, **e** and **f** are zoomed views of the respective plots.

3.3 Decays of the $f_0(1500)$

3.3.1 Sensitivity to $f_0(1500) \to \rho\rho$.

In the previous fits, we have allowed the $f_0(1500)$ to decay to both $\sigma\sigma$ and $\rho^+\rho^-$. We now would like to try and judge which of these decays is more significant. In order to to this we have taken the fits of section 3.2.1 where we have two f_0's and a ρ'. We have then allowed the $f_0(1500)$ to only decay to $\sigma\sigma$ (**figure15 a** and **b**) and to only decay to $\rho\rho$ (**figure15 c** and **d**) The maximums are summaraized in **table 5**. The very interesting feature of these plots is the fact that there is very clear peaking of the $f_0(1500)$ in the case of only $\sigma\sigma$ decays. This is more washed out with the addition of $\rho\rho$. When only $\rho\rho$ is considered, there is no eveidence of a peak, though there may be some small structure in the 1500 mass region. In terms of significance of the $\rho\rho$ decay, weconsider that change in $2\ln\mathcal{L}$ from only $\sigma\sigma$ to both $\rho\rho$ and $\sigma\sigma$. This is 11 for $\pi^+\pi^-\pi^\circ\pi^\circ\pi^\circ$ and 70 for $\pi^+\pi^-\pi^-\pi^\circ\pi^\circ$. The former is not at all significant, while the latter is at the edge of significance.

Data Set	$f_0(1500) \to \rho\rho$	$f_0(1500) \to \sigma\sigma$	$f_0(1500) \to \rho\rho$ and $\sigma\sigma$
$\pi^+\pi^-\pi^\circ\pi^\circ\pi^\circ$	7930	7975	7986
$\pi^+\pi^-\pi^-\pi^\circ\pi^\circ$	6230	6300	6370

Table 5: Comparison of maximum $2\ln\mathcal{L}$ for the $\rho\rho$ and $\sigma\sigma$ decays of the $f_0(1500)$. Note that in the case of only $\rho\rho$, the maximum is **not** at the mass and width of the $f_0(1500)$.

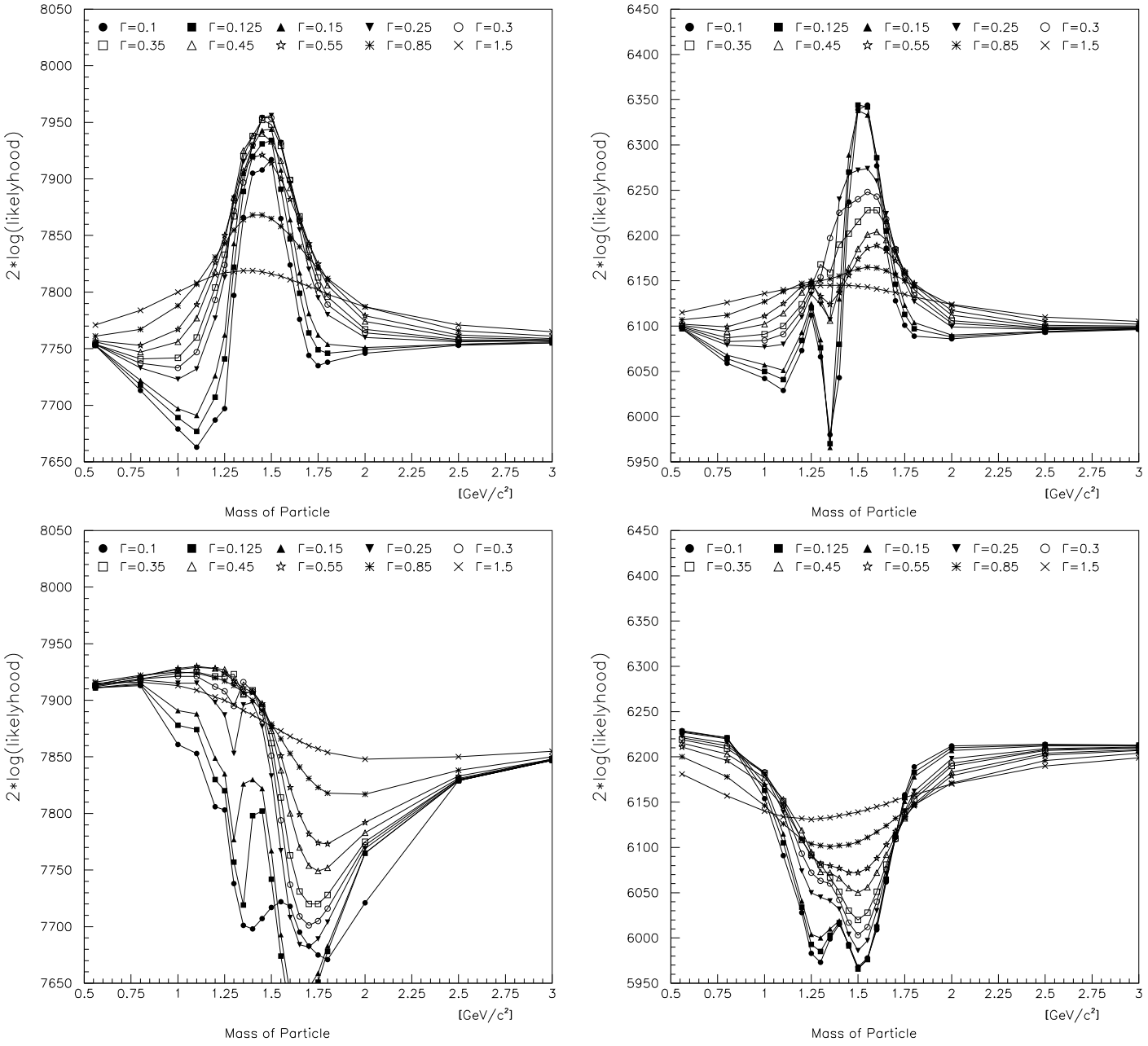

Figure 15: Fix the ρ' at $m = 1.411$, $\Gamma = 0.343$, the first f_0 to $m = 1.325$ and $\Gamma = 0.325$ and then scan the mass and width of the second f_0 resonance. **(a)** $\bar{p}p \to \pi^+\pi^-\pi^\circ\pi^\circ\pi^\circ$, with $f_0(1500) \to \sigma\sigma$. **(b)** $\bar{p}n \to \pi^+\pi^-\pi^-\pi^\circ\pi^\circ$, with $f_0(1500) \to \sigma\sigma$. **(c)** $\bar{p}p \to \pi^+\pi^-\pi^\circ\pi^\circ\pi^\circ$, with $f_0(1500) \to \rho^+\rho^-$. **(d)** $\bar{p}n \to \pi^+\pi^-\pi^-\pi^\circ\pi^\circ$, with $f_0(1500) \to \rho^+\rho^-$.

3.3.2 Sensitivity to $f_0(1500) \to \pi'(1300)\pi$.

In the publication on $5\pi^\circ$, we claim to have observed the decay of the $f_0(1500)$ into $\pi'\pi$. It is now interesting to try and determine our sensitivity to this decay path. We have taken fit 2 and fixed the two f_0 states to $m = 1.325$, $\Gamma = 0.325$ and $m = 1.500$, $\Gamma = 0.150$. We fixed the ρ' to $m = 1.411$ and $\Gamma = 0.343$. Now we allow a $\pi'\pi$ decay of the $f_0(1500)$, where the π' then decays into $\sigma\pi$. Finally, we have scanned the mass and width of the π' state. To date, we have only considered the the $\pi^-4\pi^\circ$ (12 combinations) and the $5\pi^\circ$ (60 combinations) data sets. The results of the $\log\mathcal{L}$ scans are shown in **figure 16**. The $\pi^-4\pi^\circ$ data set shows a clear peak with a mass in the range of $m = 1.175$ to $m = 1.275$, and a width between $\Gamma = 0.250$ and $\Gamma = 0.550$. The $5\pi^\circ$ data set shows a peculiar double–bump structure. The higher mass bump is clearly not understood, but assuming that the lower mass bump is the π', then we find a mass bewteen $m = 1.075$ and $m = 1.250$, with a width between $\Gamma = 0.250$ and $\Gamma = 0.550$. Clearly additional checks on the other data samples are necesary, but there does appear to be good evidence for this decay from the $\Delta\log\mathcal{L} = 250$ in the $\pi^-4\pi^\circ$ data set. This is about 400 improvement over the fit without this decay in $\pi^-4\pi^\circ$, and 90 imporvement in $5\pi^\circ$.

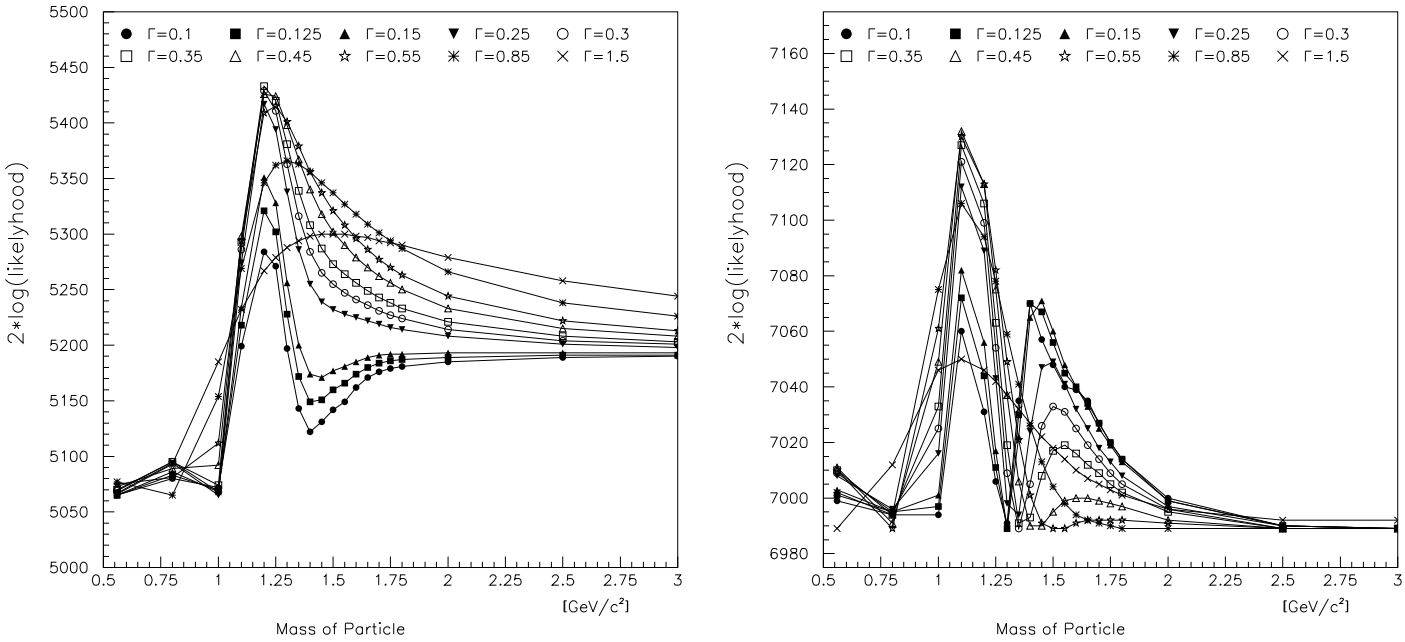

Figure 16: Scan the mass and width of the $\pi'(1300)$ from the decay of the $f_0(1500) \to \pi'\pi$ where $\pi' \to \sigma\pi$. Fix the ρ' at $m = 1.411$, $\Gamma = 0.343$ and the two f_0's at $m = 1.325$, $\Gamma = 0.325$ and $m = 1.500$, $\Gamma = 0.150$. **(a)** $\bar{p}n \to \pi^-\pi^\circ\pi^\circ\pi^\circ\pi^\circ$, and **(b)** $\bar{p}p \to \pi^\circ\pi^\circ\pi^\circ\pi^\circ\pi^\circ$.

3.4 Statistics

The number of events is also important in the analysis, particularly so in in the most complicated channel, $\pi^+\pi^-\pi^\circ\pi^\circ\pi^\circ$. Here we show in **figure 17** The effect on fit 2 when we vary the number of data and Monte Carlo events. The main question to answer here is what is the appropriate number of Monte Carlo events for doing the normalization. If we have too few events, we will be fiting statistical fluctuations in the Monte Carlo, while too many events will make the fits unmanagable. Given the formulation of the $\log\mathcal{L}$ function, we would expect the $\log\mathcal{L}$ to be proportional to the number of events if we are insensitive to both Monte Carlo and data fluctuations. Historically, a rule of thumb has been twice as much Monte Carlo as real data. In fact there is certainly also a minimum number of Monte Carlo events needed.

In the following plots, we have taken the $\pi^+\pi^-\pi^\circ\pi^\circ\pi^\circ$ data and fit it using fit number 2. We hold the mass and width of one f_0 to $m = 1.325$ and $\Gamma = 0.325$, and the mass and width of the ρ' fixed at $m = 1.411$ and $\Gamma = 0.343$. The mass and width of the second f_0 are then scanned. We have considered the event samples given in **table 3.4** and the results of these scans are shown in **figure 17** and **figure 18**.

Sample	Data	Monte Carlo	$2\log\mathcal{L}$	$2\log\mathcal{L}/N_d$
a	11445	19284	7985	0.698
b	11445	40000	8000	0.699
c	20000	40000	13865	0.693
d	39000	78000	25760	0.661

The first thing to observe is the difference between samples **a** and **b**. The former is more susceptible to statistical fluctuations in the peak region. It is quite difficult to disentangle what is happening. Sample **b** is more stable , and the peak near $f_0(1500)$ is better defined. The conclusion to draw here is that the 19284 event Monte Carlo sample is too small, and 40000 is probably a better number.

Next we compare samples **b** and **c**. Sample **c** is more stable in the peak region, and the $f_0(1500)$ is more significant above the surrounding data. Additionally, we may see what appears to be a double–peak in the $m = 1.2$ to $m = 1.5$ region. This is smeared out in sample **b**. We should conclude that for the number of parameters in this fit, the 11445 event data sample is too small. We need the 20000 data events in sample **c** to resolve details. Finally comparing samples **c** and **d**, we find very few differences. **d** is a bit sharper and cleaner, but there is no new information beyond sample **c**.

If we now look at the $\log\mathcal{L}/N_d$ in **table 3.4**, we observe a function nearly proportional to N_d. This is what we should observe. Note however that the highest statistics point is a bit low. This is not completely understood and needs to be studied in more detail. The good point is that for samples **a** and **b** which have the same number of data events, $\log\mathcal{L}/N_d$ is basically the same.

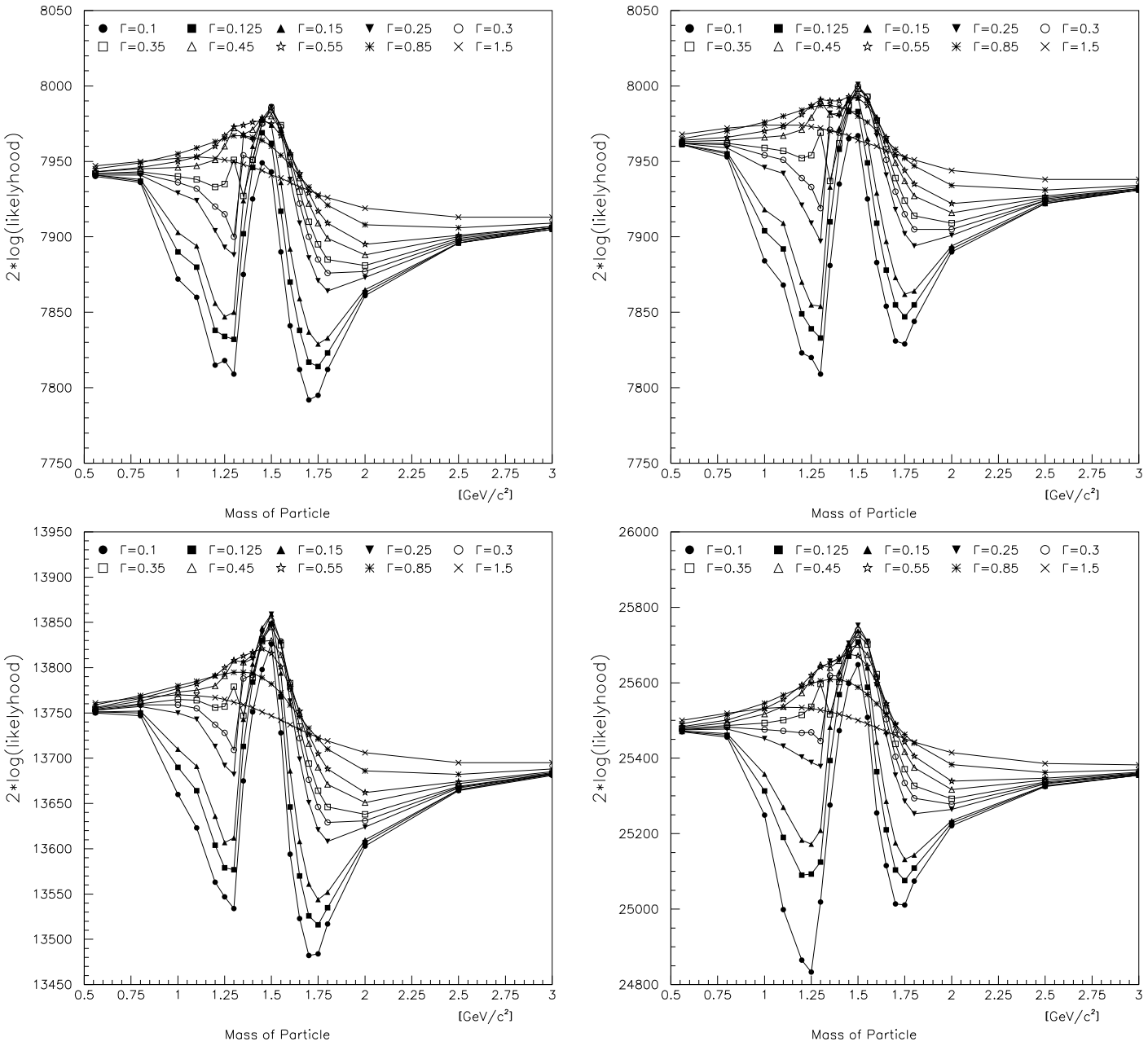

Figure 17: Fix the masses and widths for the first f_0's at $m = 1.325$, $\Gamma = 0.325$, and the ρ' at $m = 1.411$, $\Gamma = 0.343$. Scan the mass and width of the second f_0 resonance. $\bar{p}p \to \pi^+\pi^-\pi^\circ\pi^\circ\pi^\circ$ data **(a)** for 11445 data and 19284 Monte Carlo events, **(b)** for 11445 data and 40000 Monte Carlo events, **(c)** for 20000 data and 40000 Monte Carlo events, and **(d)** for 39000 data and 78000 Monte Carlo events.

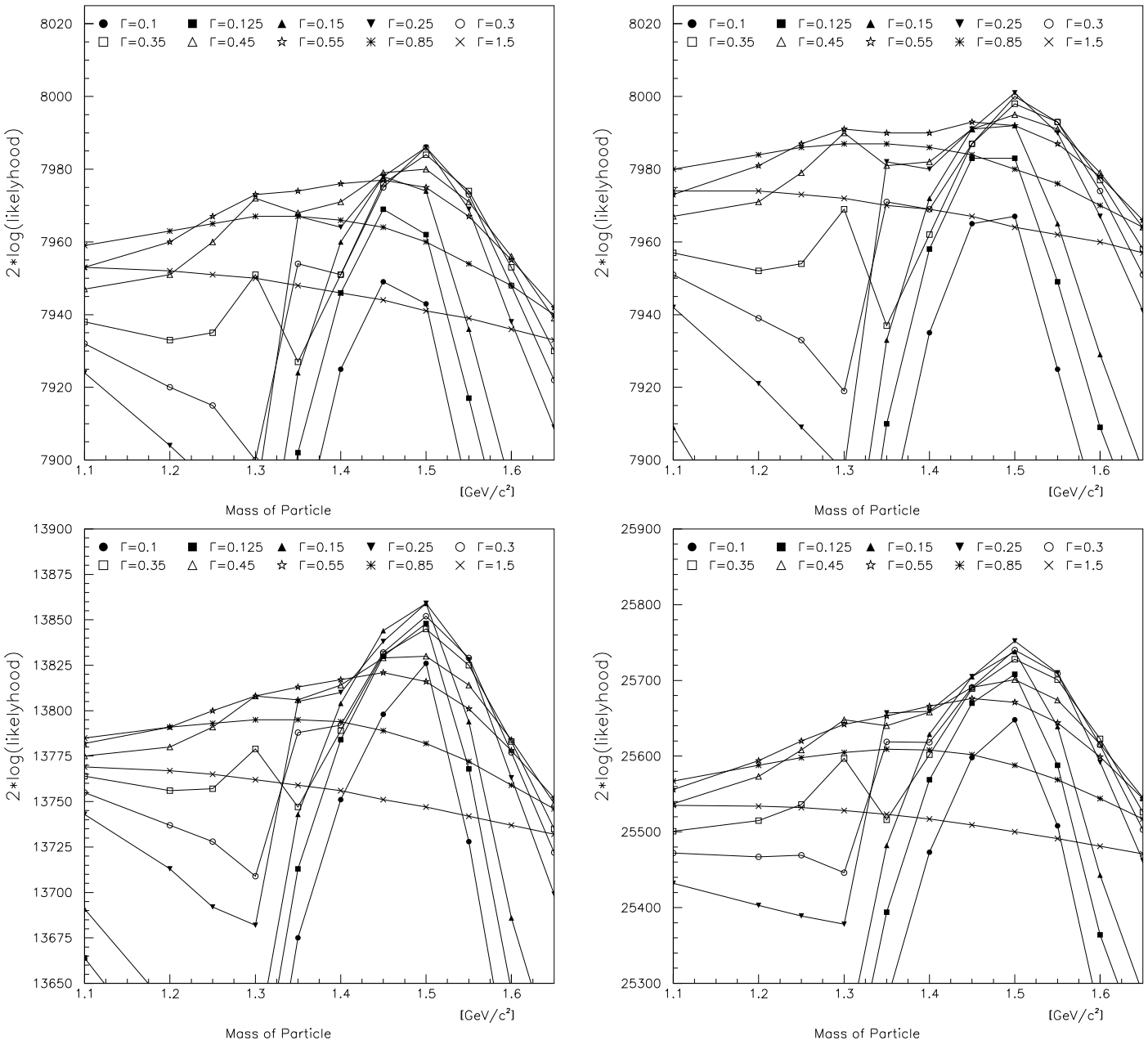

Figure 18: Fix the masses and widths for the first f_0's at $m = 1.325$, $\Gamma = 0.325$, and the ρ' at $m = 1.411$, $\Gamma = 0.343$. Scan the mass and width of the second f_0 resonance. $\bar{p}p \to \pi^+\pi^-\pi^\circ\pi^\circ\pi^\circ$ data **(a)** for 11445 data and 19284 Monte Carlo events, **(b)** for 11445 data and 40000 Monte Carlo events, **(c)** for 20000 data and 40000 Monte Carlo events, and **(d)** for 39000 data and 78000 Monte Carlo events.

3.5 The ρ' Signal

Returning to the ρ' scan in section 3.2.2, we would now like to better understand the nature of the 1^{--} wave in our data.

3.5.1 Two $\rho' \to \rho\sigma$

Looking at **figure 19 a**, which is a copy of **figure 9 a**, we notice two significant features. First, the $\log\mathcal{L}$ varies from 4500 to 9500, with a striking dip for narrow widths near $m = 1.7$. Second, there appears to be a structure near $m = 1.3$ which is washed out as the width is increased. These taken together lead us to speculate that the data demand more than one ρ'. To test this, we have introduced two ρ''s, each of which decays to $\rho\sigma$. We begin by fixing the mass and width of the first to $m = 1.411$ and $\Gamma = 0.343$. In **figure 19 b** we show the mass and width scan of the second ρ'.

There are three important changes to note. First the overall $\log\mathcal{L}$ has improved from 9200 to 9550. Next, the range of $\log\mathcal{L}$ has been decreased from 5000 to 1200. Finally, the buried structure near $m = 1.3$ has been removed, but we do have a small structure near $m = 1.5$. All three of these changes indicate that we have done the correct thing. The domiant ρ' remains the broad background term, $m = 0.560$, $\Gamma = 1.500$, but the introduction of a second ρ' with the mass and width of the $\rho'(1450)$ has improved the overall fit.

Next, we will fix the first ρ' parameters to $m = 0.560$, $\Gamma = 1.50$, and scan the second ρ'. Because of statistics problems with this fit, we have now increased the event samples from 11445 data and 20000 Monte Carlo to 20000 data and 40000 Monte Carlo. In **figure 20** we show the results of this scan **b** compared to the previous scan **a** using the same statistics. Scanning the ρ' yields a maximum $2\log\mathcal{L} = 16425$ at $m = 1.6$ and $\Gamma = 0.350$. The actual peak could be between $m = 1.45$ and $m = 1.65$ with a width between $\Gamma = 0.250$ and $\Gamma = 0.550$. The main point here is that there is a peak in this latter scan, but that the ρ' associated with it is weaker than the background term. Additionally, the structure as we approach the peak position from below may indicate the presence of a third ρ'. The data are not inconsistent with the two ρ''s of the $\pi^-\pi^\circ\pi^\circ$ analysis plus a broad background term. It will be necessary to understand this background before much more can be said about the ρ'.

3.5.2 The $\rho' \to \rho\rho$ Decay

Since we have now allowed ourselves the privilage of looking at 39000 data and 78000 Monte Carlo events in the $\pi^+\pi^-\pi^\circ\pi^\circ\pi^\circ$ data set, we would like to introduce a second decay of the ρ' into $\rho\rho$. In this data set, we now allow:

$$
\begin{aligned}
{}^1S_0(\bar{p}p) &\to \overbrace{\rho'^{\pm}\pi^{\mp}}^{L=1} \to \overbrace{\rho^{\pm}\sigma}^{L=0,S=0}\ \pi^{\mp} \\
{}^1S_0(\bar{p}p) &\to \overbrace{\rho'^{\pm}\pi^{\mp}}^{L=1} \to \overbrace{\rho^{\pm}\sigma}^{L=2,S=0}\ \pi^{\mp} \\
{}^3S_1(\bar{p}p) &\to \overbrace{\rho'^{\pm}\pi^{\mp}}^{L=1} \to \overbrace{\rho^{\pm}\sigma}^{L=0,S=0}\ \pi^{\mp} \\
{}^3S_1(\bar{p}p) &\to \overbrace{\rho'^{\circ}\pi^{\circ}}^{L=1} \to \overbrace{\rho^{\circ}\sigma}^{L=0,S=0}\ \pi^{\circ}
\end{aligned}
$$

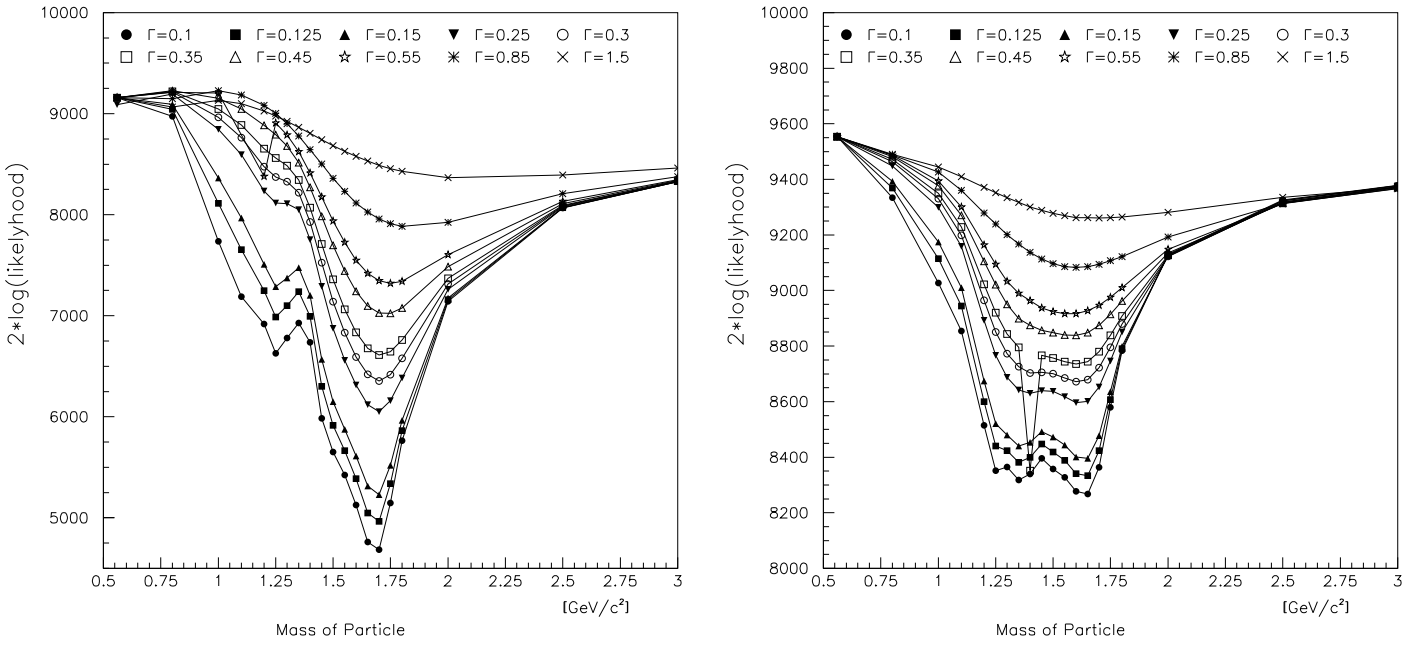

Figure 19: Fix the masses and widths for the two f_0's at $m = 1.325$, $\Gamma = 0.325$, and $m = 1.500$, $\Gamma = 0.150$. Scan the mass and width of the ρ' resonance in the $\bar{p}p \to \pi^+\pi^-\pi^\circ\pi^\circ\pi^\circ$, data sample. **(a)** Shows the scan for a single ρ'. **(b)** Shows the scan for two ρ'. One is fixed at $m = 1.411$, $\Gamma = 0.343$, and the second is scanned.

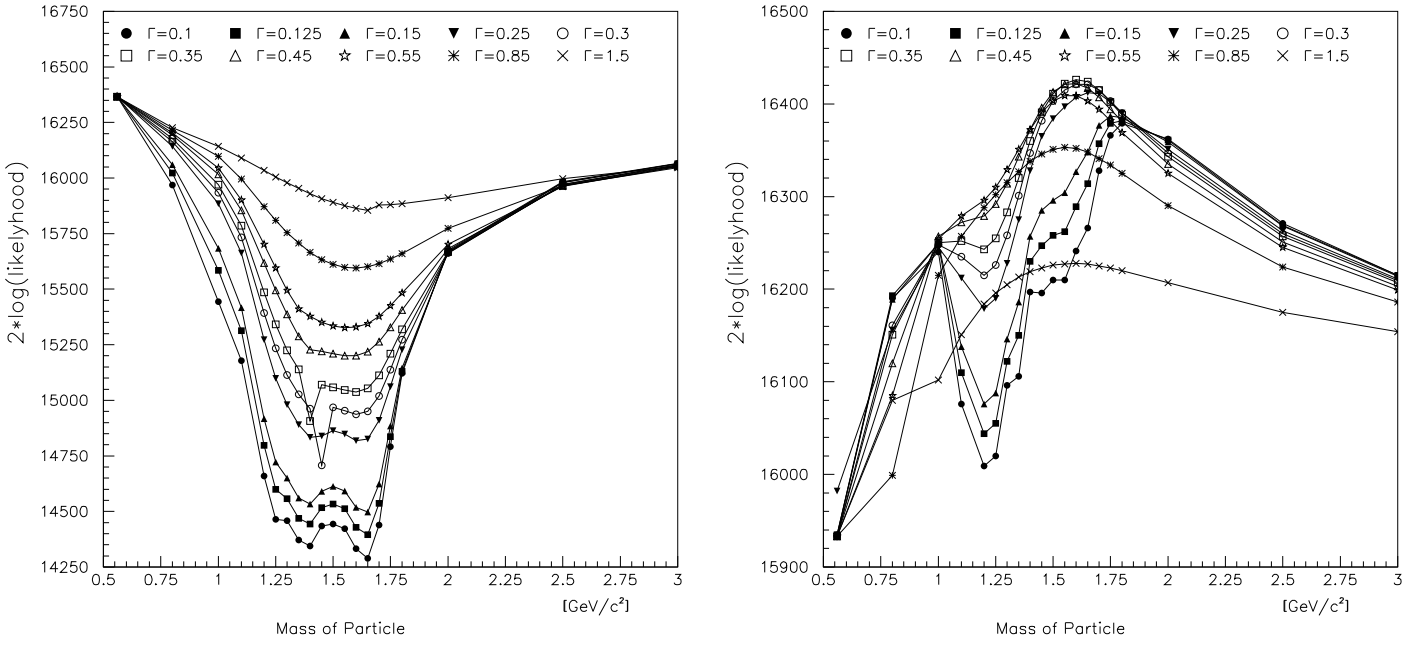

Figure 20: Fix the masses and widths for the two f_0's at $m = 1.325$, $\Gamma = 0.325$, and $m = 1.500$, $\Gamma = 0.150$. Scan the mass and width of the ρ' resonance in the $\bar{p}p \to \pi^+\pi^-\pi^\circ\pi^\circ\pi^\circ$, data sample. **(a)** Shows the scan for two ρ'. One is fixed at $m = 1.411$, $\Gamma = 0.343$, and the second is scanned. **(b)** Shows the scan for two ρ'. One is fixed at $m = 0.560$, $\Gamma = 1.5$, and the second is scanned.

$$
\begin{aligned}
{}^3S_1(\bar{p}p) &\rightarrow \overbrace{\rho'^{\pm}\pi^{\mp}}^{L=1} \rightarrow \overbrace{\rho^{\pm}\sigma}^{L=2,S=0}\ \pi^{\mp} \\
{}^3S_1(\bar{p}p) &\rightarrow \overbrace{\rho'^{\circ}\pi^{\circ}}^{L=1} \rightarrow \overbrace{\rho^{\circ}\sigma}^{L=2,S=0}\ \pi^{\circ} \\
{}^3S_1(\bar{p}p) &\rightarrow \overbrace{\rho'^{\circ}\pi^{\circ}}^{L=1} \rightarrow \overbrace{\rho^{+}\rho^{-}}^{L=1,S=0}\ \pi^{\circ} \\
{}^3S_1(\bar{p}p) &\rightarrow \overbrace{\rho'^{\circ}\pi^{\circ}}^{L=1} \rightarrow \overbrace{\rho^{+}\rho^{-}}^{L=1,S=1}\ \pi^{\circ} \\
{}^3S_1(\bar{p}p) &\rightarrow \overbrace{\rho'^{\circ}\pi^{\circ}}^{L=1} \rightarrow \overbrace{\rho^{+}\rho^{-}}^{L=1,S=2}\ \pi^{\circ}
\end{aligned}
$$

Because of the final state, the new decay must couple to $\rho^+\rho^-$, or must be ρ'°. This can only couple to negative C–parity initial state, or ${}^3S_1$. In the $\pi^+\pi^-\pi^-\pi^\circ\pi^\circ$ data set, we could couple to the ${}^1S_0$ initial state via:

$$
\begin{aligned}
{}^1S_0(\bar{p}n) &\rightarrow \overbrace{\rho'^{\circ}\pi^{-}}^{L=1} \rightarrow \overbrace{\rho^{+}\rho^{-}}^{L=1,S=0}\ \pi^{-} \\
{}^1S_0(\bar{p}n) &\rightarrow \overbrace{\rho'^{\circ}\pi^{-}}^{L=1} \rightarrow \overbrace{\rho^{+}\rho^{-}}^{L=1,S=1}\ \pi^{-} \\
{}^1S_0(\bar{p}n) &\rightarrow \overbrace{\rho'^{\circ}\pi^{-}}^{L=1} \rightarrow \overbrace{\rho^{+}\rho^{-}}^{L=1,S=2}\ \pi^{-}
\end{aligned}
$$

but due to the limited statistics currently available in these data, this has not been tested.

In **figure 21** we show the scan of the mass and width of the ρ'. In order to determine if this is significant, we need to compare with the high statistics point in **figure 18** which was scanned for a ρ' at $m = 1.411$, $\Gamma = 0.343$, and has a maximum at $2\log\mathcal{L} = 25740$ for the $f_0(1500)$. **Figure 21** has $2\log\mathcal{L} = 26400$ for the ρ' curve. While this change of 660 in $2\log\mathcal{L}$ is significant, we can probably say little more until we better understand the ρ' in these data.

4 Conclusions

There are several conclusions which can be drawn from this report. We begin with the statistics of the Monte Carlo sample. In most cases, 20000 will be insufficient to properly integrate over the 8–D phase space. Our feeling here is that 40000 events is probably sufficient. Early, we felt that one should have twice as much Monte Carlo as data. This may not be true and should be tested further. Reducing the total Monte Carlo from 80000 to 40000 will significantly reduce the computer resources needed to perform the fits.

In regard to the data sets, we find that the $\pi^+\pi^-\pi^\circ\pi^\circ\pi^\circ$ data set has little sensitivity to the exact nature of the f_0 states though it clearly shows the $f_0(1500)$. Perhaps as a larger fraction of the final state is understood, the sensitivity will improve. However, this channel should not currently be used to extract these parameters. These data do have the most sensitivity to the ρ'. This is mostly due to its production in the ${}^3S_1$ initial state to which this channel can couple. These data are probably the best place to extract information on the ρ' from the 5π samples.

The $\pi^-\pi^\circ\pi^\circ\pi^\circ\pi^\circ$ data set appears to have the greatest sensitivity to the f_0 states. This is probably due to the minimum number of combinatorics involved. This is likely to be the best data for extracting the f_0 parameters, and probably its $\sigma\sigma$ coupling. It clearly shows the most

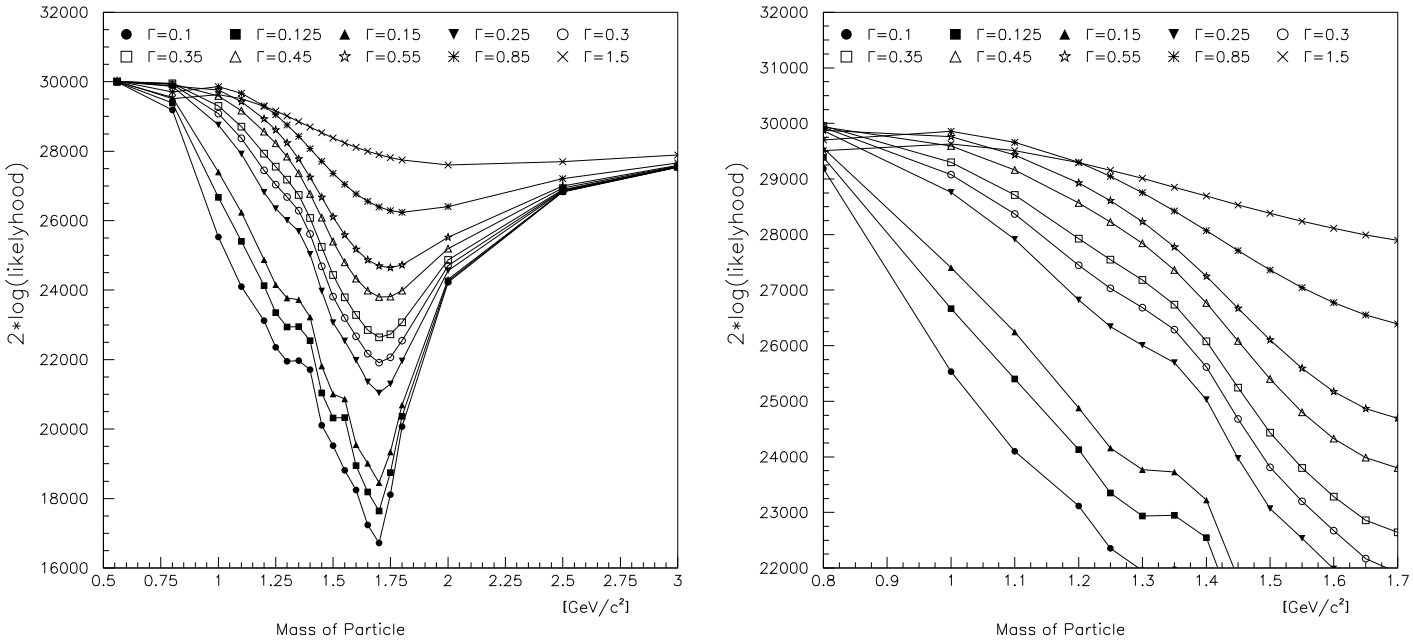

Figure 21: Fix the masses and widths of the two f_0 states to $m = 1.325$, $\Gamma = .325$ and $m = 1.500$, $\Gamma = 0.150$ and then scan the mass and width of ρ'. This ρ' is allowed to decay to both $\rho(770)\sigma$ and $\rho^+\rho^-$.

striking evidence of any data set for the $f_0(1500)$. These data are also sensitive to the $\pi'(1300)\pi$ decay of the $f_0(1500)$, where $\pi'(1300) \to \sigma\pi$. However, these data tell us nothing about the $\rho\rho$ couplings of these states. The $\pi^+\pi^-\pi^-\pi^\circ\pi^\circ$ data set may be the next most sensitive to the f_0 and will also give us access to the $\rho^+\rho^-$ couplings of these states. It is also likely to be these data that shed additional light on the $\pi'(1300)\pi$ decay of the f_0 states — particularly if the $\pi'(1300) \to \rho(770)\pi$ decay exists.

Finally, the $5\pi^0$ data with their rather large combinatorics will certainly provide additional constraints on the f_0 states. Given the very limited number of initial states, it will be quite important that any description of the data be able to explain these data as well. However, given the ambiguities in the earlier publication, these data alone are not going to be able to resolve the f_0's.

As a plan for proceeding with the analysis is first to increase all Monte Carlo samples to at least 40000 events. In addition, the April '96 data will be processed to increase the $\pi^+\pi^-\pi^-\pi^\circ\pi^\circ$ sample to about 25000 events. We should then aim for a combined analysis using about 25000 events from each channel. In addition, we feel that the $\pi^-4\pi^\circ$ data alone make a very convincing case for the 4π decay of the $f_0(1500)$. While we may be unable to settle the exact fraction of $\pi'(1300)\pi$, the $f_0(1500)$ does stand out like a *sore thumb*. These data should probably be used to make a single–channel Physics Letters article concentrating on the $f_0(1500)$. The combined data sets should then be used to write a long Physical Review D article which would explain in detail how the fits work, the common features of the data, and how all of this relates to earlier 5π analyses.

References

[1] S. U. Chung, J. Brose, R. Hackmann, E. Klempt, S. Spanier and C. Strassburger, Ann. d. Physik **4**, 404, (1995).

[2] S. Spanier, CB–Note 274.

[3] C. A. Meyer, CB–Note 221.

[4] C. Strassburger, CB–Note 297.